Iodinated Salicylhydrazone Derivatives as Potent α-Glucosidase Inhibitors: Synthesis, Enzymatic Activity, Molecular Modeling, and ADMET Profiling

Seema K. Bhagwat [1,†], Fabiola Hernandez-Rosas [2,3,4,†], Abraham Vidal-Limon [5], J. Oscar C. Jimenez-Halla [6], Balasaheb K. Ghotekar, [1] Vivek D. Bobade, [1] Enrique Delgado-Alvarado,[7] Sachin V. Patil [1,*]and Tushar Janardan Pawar [5,8,*]

[1] *Department of Chemistry, Research Centre HPT Arts and RYK Science College (Affiliated to S. P. Pune University), Nashik, 422005, Maharashtra, India; sachin.dhokare@gmail.com*
[2] *Centro de Investigacion, Universidad Anahuac Queretaro, El Marques, Queretaro 76246, Mexico; fabiola.hernandezro@anahuac.mx*
[3] *Escuela de Ingenieria Biomedica, Division de Ingenierias, Universidad Anahuac Queretaro, El Marques, Queretaro 76246, Mexico*
[4] *Facultad de Quimica, Universidad Autonoma de Queretaro, Queretaro 76010, Mexico.*
[5] *Red de Estudios Moleculares Avanzados, Instituto de Ecología, A. C., Carretera Antigua a Coatepec 351, 91073, Xalapa, Veracruz, México; tushar.janardan@inecol.mx*
[6] *Departamento de Química, División de Ciencias Naturales y Exactas, Universidad de Guanajuato, Noria Alta S/N, 36050, Guanajuato, Guanajuato, México.; jjimenez@ugto.mx*
[7] *Micro and Nanotechnology Research Center, Universidad Veracruzana, Blvd. Av. Ruiz Cortines No. 455 Fracc. Costa Verde, Boca del Río, Veracruz 94294, México; endelgado@uv.mx*
[8] *Unidad de Desarrollo e Investigación en Bioterapeúticos (UDIBI), Escuela Nacional de Ciencias Biológicas, Instituto Politécnico Nacional, 11340 Mexico City, Mexico.*

Corresponding Authors:

Tushar Janardan Pawar (Email: tushar.janardan@inecol.mx)*

Sachin V. Patil (Email: sachin.dhokare@gmail.com)*

Table of Content

1.	General Methods	S3
2.	Synthesis and Characterization	S4
3.	Biological Assay	S9
4.	DFT Study	S13
5.	Molecular Dynamics Simulations	S23
6.	Statistical Analysis and Visualizations	S27
7.	SAR Analysis	S36
8.	NMR and Mass Spectra	S52
9.	References	S77

1. General Methods

All reactions were performed under a dry nitrogen atmosphere. Chemicals and reagents, including solvents such as ethanol (EtOH, 99.5%), were purchased from Sigma-Aldrich and used without further purification. Glassware was oven-dried prior to use, and heating reactions were conducted in a paraffin oil bath.

Thin-layer chromatography (TLC) was performed on pre-coated aluminum plates of silica gel 60 F254 (0.25 mm, E. Merck). Plates were visualized under a short-wave UV lamp and by heating after dipping in a ninhydrin solution. Column chromatography was conducted using silica gel (100–200 mesh and 230–400 mesh), with eluents chosen based on polarity correlated to TLC mobility.

NMR spectroscopy was conducted using a Bruker Avance III 600 MHz spectrometer with deuterated dimethyl sulfoxide (DMSO-d6, 99.8%) as the solvent. Chemical shifts (δ) are reported in parts per million (ppm) relative to solvent peaks. Proton assignments were confirmed using ^{1}H-^{1}H COSY experiments, and ^{1}H-^{13}C HSQC experiments were performed to establish proton-carbon correlations. Data for ^{1}H NMR are reported as follows: chemical shift (δ, ppm), multiplicity (s: singlet, d: doublet, dd: doublet of doublets, t: triplet, q: quartet, m: multiplet, brs: broad singlet, ABq: AB quartet), coupling constant (J in Hz), integration, and assigned protons.

Mass spectra were acquired using a TOF/TOF™ Reflector mass spectrometer, and the raw data were processed using the associated software. The spectra provided high-resolution mass measurements, aiding in the confirmation of molecular structures.

2. Synthesis and Characterization

2.1. Synthesis of 5-iodo-2-salicylic ester (2)

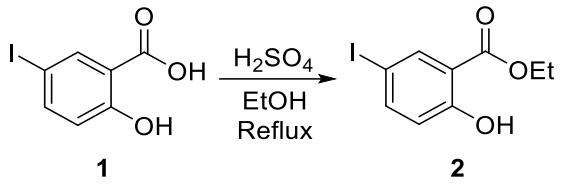

1 2

5-iodo-salicylic acid compound **1** (2 g, 7.57 mmol) was dissolved in Ethanol (40 mL). After stirring the reaction mixture at room temperature for 10 min, 1 M H_2SO_4 (0.56 mL) was added dropwise and refluxed at 90 °C for 18 h. Reaction mixture was diluted with EtOAc (40 mL) and washed successively with aq. $NaHCO_3$. The separated organic layer was dried over Na_2SO_4, concentrated and purified by column chromatography (100-200 mesh, 20% EtOAc-petroleum ether) on silica gel to afford 5-iodo-salicylic acid -ester compound **2** as white solid (1.64 g, 74.14%). **^{1}H NMR (600 MHz, DMSO-*d*$_6$)**: δ 10.56 (s, 1H), 7.99 (d, J = 2.3 Hz, 1H), 7.77 (dd, J = 8.7, 2.3 Hz, 1H), 6.82 (d, J = 8.7 Hz, 1H), 4.34 (q, J = 7.1 Hz, 2H), 1.33 (t, J = 7.1 Hz, 3H). **^{13}C NMR (151 MHz, DMSO-*d*$_6$)**: δ 167.72, 159.99, 143.86, 138.21, 120.59, 116.44, 81.35, 62.08, 14.42. **HRMS (TOF) (m/z)**: $[M + H]^+$ calcd for $C_9H_9IO_3$ 291.9596; found 291.9572.

2.2. Synthesis of 5-iodo-2-hydroxybenzo-hydrazide (3)

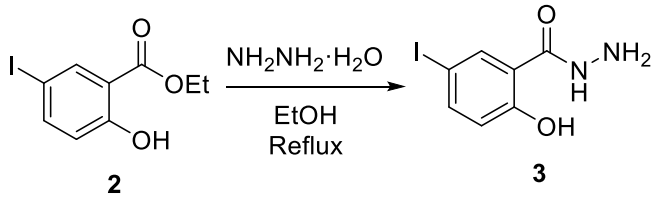

2 3

A mixture of 5-iodo-ethyl salicylate **2** (10 mM) and hydrazine hydrate (20 mM) was heated under reflux in 50 mL of 95% ethanol for 15 h, then the reaction mixture was concentrated and poured

onto crushed ice. The separated crude solid was filtered off, washed successively with water, dried and recrystallized from ethanol to give **3** as colorless crystals. **^{1}H NMR (600 MHz, DMSO-*d*$_6$):** δ 10.07 (s, 1H), 8.12 (d, J = 2.2 Hz, 1H), 7.65 (dd, J = 8.6, 2.2 Hz, 1H), 6.75 (d, J = 8.6 Hz, 1H). **^{13}C NMR (151 MHz, DMSO-*d*$_6$):** δ 166.62, 159.39, 141.79, 135.99, 120.39, 116.44, 80.98. **HRMS (TOF) (m/z)**: $[M + H]^+$ calcd for $C_7H_7IN_2O_2$ 277.9552; found 277.9557.

2.3. General procedure for preparation of hydrazone derivatives (4a-j)

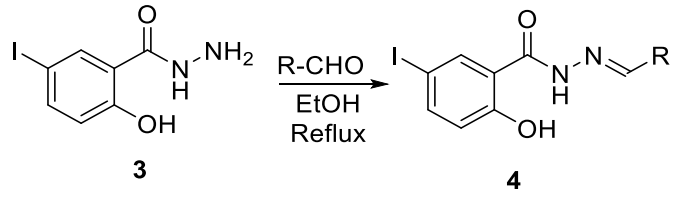

3 4

A mixture of the appropriate 5-iodo-2-hydroxybenzohydrazide **2** (10 mM), benzaldehyde derivatives (10 mM) in absolute ethanol (10 mL) and a few drops of acetic acid was refluxed for 5–9 h, the reaction mixture was left to attain room temperature, and the solid matter that separated was filtered off and recrystallized from ethanol to give hydrazones.

(E)-2-hydroxy-5-iodo-N'-(thiazol-2-ylmethylene)benzohydrazide (4a): White solid (68 %);

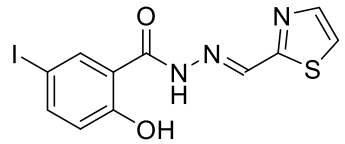

4a

^{1}H NMR (600 MHz, DMSO-*d*$_6$): δ 12.06 (s, 1H), 11.60 (s, 1H), 8.66 (s, 1H), 8.08 (d, J = 2.3 Hz, 1H), 8.00 (d, J = 3.2 Hz, 1H), 7.89 (d, J = 3.2 Hz, 1H), 7.73 (dd, J = 8.6, 2.3 Hz, 1H), 6.84 (d, J = 8.6 Hz, 1H). **^{13}C NMR (151 MHz, DMSO-*d*$_6$):** δ 164.40, 163.48, 158.33, 144.64, 143.41, 142.28, 137.32, 122.85, 120.29, 120.08, 81.45. **HRMS (TOF) (m/z)** : $[M + H]^+$ calcd for $C_{11}H_8IN_3O_2S$ 372.9382; found 372.9389.

(E)-2-hydroxy-5-iodo-N'-(pyridin-3-ylmethylene)benzohydrazide (4b): White solid (78%);

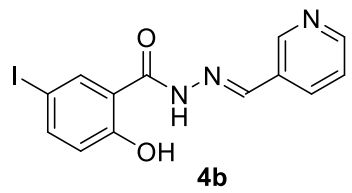

4b

^{1}H NMR (600 MHz, DMSO-*d*$_6$): δ 11.96 (s, 1H), 11.80 (s, 1H), 8.88 (d, J = 2.2 Hz, 1H), 8.64 (dd, J = 4.8, 1.7 Hz, 1H), 8.50 (s, 1H), 8.20 – 8.12 (m, 2H), 7.73 (dd, J = 8.7, 2.2 Hz, 1H), 7.51 (dd, J = 8.0, 4.8 Hz, 1H), 6.84 (d, J = 8.7 Hz, 1H). **^{13}C NMR (151 MHz, DMSO-*d*$_6$):** δ 163.60, 158.68, 151.45, 149.40, 146.70, 142.24, 137.21, 134.09, 130.44, 124.55, 120.36, 119.64, 81.42. **HRMS (TOF) (m/z)** : $[M + H]^+$ calcd for $C_{13}H_{10}IN_3O_2$ 366.9818; found 366.9836.

(E)-2-hydroxy-N'-(4-hydroxy-3-nitrobenzylidene)-5-iodobenzohydrazide (4c): yellow solid

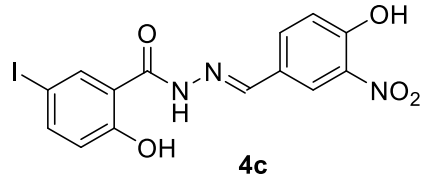

4c

(75%); **^{1}H NMR (600 MHz, DMSO-*d*$_6$):** δ 11.86 (s, 2H), 11.59 (s, 1H), 8.40 (s, 1H), 8.22 (d, J = 2.3 Hz, 1H), 8.15 (d, J = 2.3 Hz, 1H), 7.99 – 7.90 (m, 1H), 7.76 – 7.67 (m, 1H), 7.23 (d, J = 8.5 Hz, 1H), 6.83 (d, J = 8.5 Hz, 1H). **^{13}C NMR (151 MHz, DMSO-*d*$_6$):** δ 163.53, 158.78, 154.04, 147.41, 142.19, 137.55, 137.10, 133.49, 125.95, 124.80, 120.35, 120.23, 119.48, 81.39. **HRMS (TOF) (m/z)** : $[M + H]^+$ calcd for $C_{14}H_{10}IN_3O_5$ 426.9665; found 426.9654.

(E)-2-hydroxy-5-iodo-N'-(4-nitrobenzylidene)benzohydrazide (4d): Yellow solid (78%); **^{1}H**

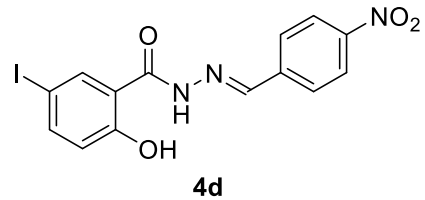

4d

NMR (600 MHz, DMSO-*d*$_6$): δ 12.04 (s, 1H), 11.73 (s, 1H), 8.54 (s, 1H), 8.31 (d, J = 8.6 Hz, 2H), 8.13 (d, J = 2.3 Hz, 1H), 8.00 (d, J = 8.5 Hz, 2H), 7.73 (dd, J = 8.6, 2.3 Hz, 1H), 6.84 (d, J = 8.7 Hz, 1H). **^{13}C NMR (151 MHz, DMSO-*d*$_6$):** δ 163.64, 158.50, 148.47, 146.80, 142.29, 140.80, 137.38, 128.66, 124.58, 120.32, 119.83, 81.47. **HRMS (TOF) (m/z)**: $[M + H]^+$ calcd for $C_{14}H_{10}IN_3O_4$ 410.9716; found 410.9721.

(E)-N'-(3-bromobenzylidene)-2-hydroxy-5-iodobenzohydrazide (4e): White solid (82%); **^{1}H NMR (600 MHz, DMSO-*d*$_6$):** δ 11.94 (s, 1H), 11.83 (s, 1H), 8.41 (s, 1H), 8.15 (d, J = 2.3 Hz, 1H), 7.94 (t, J = 1.8 Hz, 1H), 7.76 – 7.70 (m, 2H), 7.68 – 7.63 (m, 1H), 7.44 (t, J = 7.9 Hz, 1H), 6.84 (d, J = 8.6 Hz, 1H). **^{13}C NMR (151 MHz, DMSO-*d*$_6$):** δ 163.65, 158.71, 147.60, 142.24, 137.20, 136.96, 133.33, 131.53, 129.81, 126.85, 122.67, 120.35, 119.58, 81.41. **HRMS (TOF) (m/z)**: $[M + H]^+$ calcd for $C_{14}H_{10}IN_2O_2$ 443.8970; found 443.8959.

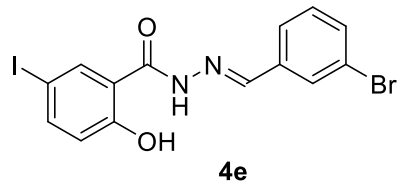

4e

(E)-2-hydroxy-N'-(4-hydroxybenzylidene)-5-iodobenzohydrazide (4f): White solid (76%); **^{1}H NMR (600 MHz, DMSO-*d*$_6$):** δ 12.07 (s, 1H), 11.70 (s, 1H), 10.00 (s, 1H), 8.34 (s, 1H), 8.18 (d, J = 2.2 Hz, 1H), 7.71 (dd, J = 8.6, 2.2 Hz, 1H), 7.59 (d, J = 8.3 Hz, 2H), 6.84 (dd, J = 24.2, 8.5 Hz, 3H). **^{13}C NMR (151 MHz, DMSO-*d*$_6$):** δ 163.57, 160.21, 159.22, 149.95, 142.14, 136.77, 129.62, 125.40, 120.42, 119.08, 116.25, 81.26. **HRMS (TOF) (m/z)**: $[M + H]^+$ calcd for $C_{14}H_{11}IN_2O_3$ 381.9814; found 381.9822.

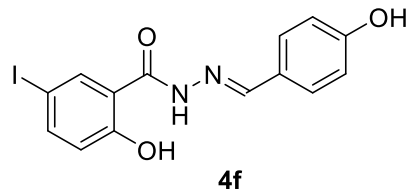

4f

(E)-N'-(2-fluorobenzylidene)-2-hydroxy-5-iodobenzohydrazide (4g): White solid (80%); **^{1}H NMR (600 MHz, DMSO-*d*$_6$):** δ 11.98 (s, 1H), 11.85 (s, 1H), 8.69 (s, 1H), 8.16 (d, J = 2.3 Hz, 1H), 7.96 (td, J = 7.6, 1.7 Hz, 1H), 7.73 (dd, J = 8.7, 2.2 Hz, 1H), 7.56 – 7.51 (m, 1H), 7.37 – 7.30 (m, 2H), 6.84 (d, J = 8.7 Hz, 1H). **^{13}C NMR (151 MHz, DMSO-*d*$_6$):** δ 163.92, 162.22, 160.56, 159.09, 142.32, 142.24, 142.21, 136.91, 132.88, 132.82, 126.94, 125.51, 122.09, 122.02, 120.42, 119.28, 116.63, 116.49, 81.31. **HRMS (TOF) (m/z)** $[M + H]^+$ calcd for $C_{14}H_{10}FIN_2O_2$ 383.9771; found 383.9770.

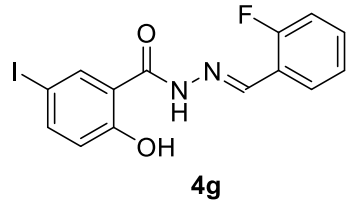

4g

(E)-2-hydroxy-N'-(2-hydroxy-4-methoxybenzylidene)-5-iodobenzohydrazide (4h): White solid (70%); **^{1}H NMR (600 MHz, DMSO-*d*$_6$):** δ 11.94 (s, 2H), 11.42 (s, 1H), 8.58 (s, 1H), 8.17 (d, J = 2.2 Hz, 1H), 7.72 (dd, J = 8.7, 2.2 Hz, 1H), 7.46 (d, J = 8.6 Hz, 1H), 6.83 (d, J = 8.7 Hz, 1H), 6.54 (dd, J = 8.6, 2.4 Hz, 1H), 6.51 (d, J = 2.5 Hz, 1H), 3.79 (s, 3H). **^{13}C NMR (151 MHz, DMSO-*d*$_6$):** δ 163.29, 162.83, 159.94, 159.10, 150.14, 142.29, 136.85, 131.48, 120.42, 118.88, 112.16, 107.11, 101.62, 81.32, 55.82. **HRMS (TOF) (m/z)** : $[M + H]^+$ calcd for $C_{15}H_{13}IN_2O_4$ 411.9920; found 411.9912.

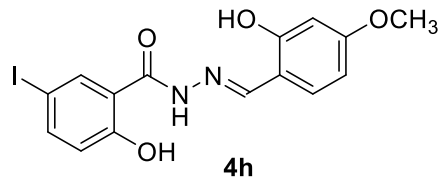

4h

(E)-2-hydroxy-5-iodo-N'-(naphthalen-2-ylmethylene)benzohydrazide (4i): White solid (71%); **^{1}H NMR (600 MHz, DMSO-*d*$_6$):** δ 11.93 (d, J = 14.5 Hz, 2H), 8.61 (s, 1H), 8.19 (d, J = 2.1 Hz, 2H), 8.05 – 8.02 (m, 1H), 8.00 (d, J = 1.2 Hz, 2H), 7.98 – 7.95 (m, 1H), 7.74 (dd, J = 8.6, 2.2 Hz, 1H), 7.60 – 7.57 (m, 2H), 6.85 (d, J = 8.6 Hz, 1H). **^{13}C NMR (151 MHz, DMSO-*d*$_6$):** δ 163.70, 158.91, 149.42, 142.21, 137.05, 134.35, 133.30, 132.24, 129.59, 129.06, 128.90, 128.29, 127.79, 127.31, 123.18, 120.39, 119.55, 81.38. **HRMS (TOF) (m/z)**: $[M + H]^+$ calcd for $C_{18}H_{13}IN_2O_2$ 416.0022; found 416.0022.

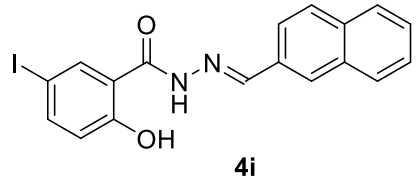

4i

(E)-N'-benzylidene-2-hydroxy-5-iodobenzohydrazide (4j): White solid (76%); **^{1}H NMR (600 MHz, DMSO-*d*$_6$):** δ 11.91 (s, 1H), 11.85 (s, 1H), 8.45 (s, 1H), 8.17 (d, J = 2.2 Hz, 1H), 7.82 – 7.67 (m, 3H), 7.48 (td, J = 5.1, 4.7, 3.0 Hz, 3H), 6.84 (d, J = 8.6 Hz, 1H). **^{13}C NMR (151 MHz, DMSO-*d*$_6$):** δ 163.67, 158.93, 149.51, 142.21, 137.04, 134.48, 130.88, 129.37, 127.77, 120.39, 119.41, 81.36. **HRMS (TOF) (m/z)** : $[M + H]^+$ calcd for $C_{14}H_{11}IN_2O_2$ 366.9865; found 366.9856.

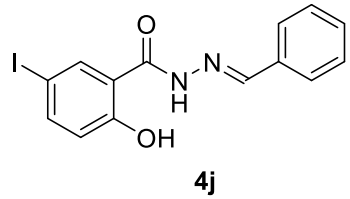

4j

3. α-Glucosidase assay

3.1. Screening of All Compounds at a Fixed Concentration

The initial screening of all compounds was carried out at a fixed concentration of 100 μM to evaluate their α-glucosidase inhibitory activity. For this purpose, 10 μL of each test sample (0.1 mM DMSO solution) was reconstituted in 70 μL of 100 mM phosphate buffer (pH 6.8) and placed in a 96-well microplate. To initiate the reaction, 10 μL of α-glucosidase enzyme solution (0.05 U/mL final well concentration) was added to each well, followed by incubation at room temperature for 15 minutes. After the incubation, 10 μL of the substrate solution (5 mM p-nitrophenyl-α-D-glucopyranoside prepared in the same buffer) was added to all wells.

The plate was incubated for 1 hour to allow the enzyme to catalyze the reaction, and the release of p-nitrophenol was monitored spectrophotometrically at 450 nm. Individual blanks were prepared for each test sample to correct background absorbance, where the substrate was replaced with 10 μL of buffer. The control sample, representing maximum enzyme activity, contained 10 μL DMSO in place of the test samples.

The percentage of enzyme inhibition was calculated using the formula:

$$\%\ Inhibition = \left(1 - \frac{Absorption_{sample}}{Absorption_{control}}\right) \times 100$$

This calculation allowed for the identification of compounds exhibiting significant α-glucosidase inhibition under uniform conditions (Table S5).

Table S1: Absorbance values (A 450 nm) for α-glucosidase inhibitory activity of test compounds (**4a**–**4j**), positive control (Acarbose), and buffer (negative control) measured in triplicate (**R1**, **R2**, **R3**). Lower absorbance values indicate higher inhibition of α-glucosidase enzyme activity.

Compounds	R1	R2	R3
4a	0.723	0.809	0.809
4b	1.086	1.128	1.196
4c	1.166	1.334	1.33
4d	0.945	0.847	1.056
4e	0.11	0.217	0.203
4f	1.067	0.959	1.111
4g	0.329	0.346	0.333
4h	2.025	2.013	2.007
4i	0.265	0.256	0.282
4j	0.13	0.108	0.202
Acarbose	0.399	0.337	0.352
Buffer	2.567	2.095	2.446

3.2. Determination of IC_{50} Values

The IC_{50} values, which represent the concentration of the compound required to achieve 50% enzyme inhibition, were determined for the most active compounds using a concentration-response assay. For this purpose, test samples were prepared at varying concentrations to generate a dose-response curve. The concentrations used were: 100, 50, 25, 12.5, 6.25, 3.125, 1.5625, and 0 µM.

Each concentration was tested in triplicate to ensure accuracy and reproducibility of the results. The assay procedure was performed under the same conditions as the initial screening: 10 µL of each test sample (prepared at the respective concentration) was incubated with 70 µL of 100 mM phosphate buffer (pH 6.8) and 10 µL of α-glucosidase enzyme solution (0.05 U/mL final well concentration) for 15 minutes. Following the incubation, 10 µL of the substrate solution (5 mM p-nitrophenyl-α-D-glucopyranoside) was added, and the plate was incubated for 1 hour. Absorbance was measured at 450 nm to quantify the enzyme activity.

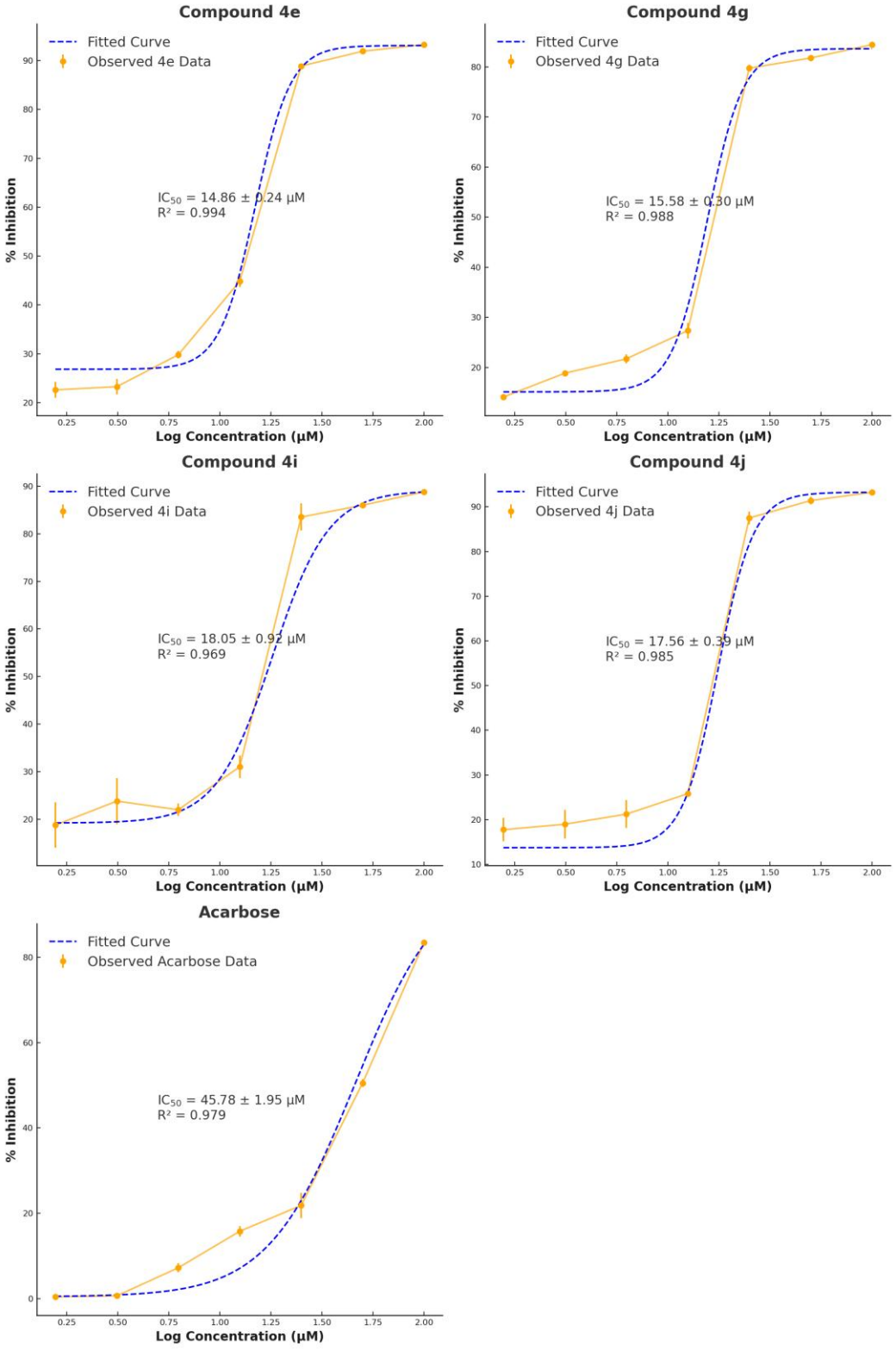

Figure S1. IC_{50} values for compounds **4e**, **4g**, **4i**, **4j** and acarbose.

Individual blanks were prepared for each concentration by replacing the substrate with buffer to correct for background absorbance. The control sample (0 μM inhibitor) contained DMSO and served as a reference for maximum enzyme activity, while acarbose was used as the positive control to validate the assay.

The percentage inhibition at each concentration was calculated using the same formula. The percentage inhibition values were plotted against the log-transformed concentrations of the compounds. Nonlinear regression analysis, using the four-parameter logistic model, was performed to fit the data and determine the IC_{50} values for the most active compounds (Figure S1).

4. DFT Study

4.1. Methodology

Theoretical calculations were performed using the Gaussian09 rev. D.01 package.[1] Gas-phase geometry optimizations were carried out (no constraints or symmetry restrictions were used) with the long-range hybrid functional ωB97X-D[2] in conjunction with Ahlrichs' def2-tzvpp basis set[3] for all the atoms. Subsequent harmonic frequency calculations were performed to corroborate the loca minimum character of each optimized species. We plotted the electrostatic potential of each compound using Gaussview program.[4] The band gap energy was calculated simply as the difference between the LUMO energy and the HOMO energy: $E_{gap} = E_{LUMO} - E_{HOMO}$ expressed in electron-volts (eV).

4.2. HOMO-LUMO Gap Analysis

Table S2. Orbital energies of HOMO and LUMO in hartrees and energy gap (in eV) calculated at the ωB97X-D/def2-tzvpp level.

Compound	HOMO	LUMO	Energy gap
4a	–0.3007	–0.0106	7.89
4b	–0.3038	–0.0066	8.09
4c	–0.3002	–0.0342	7.24
4d	–0.3137	–0.0343	7.60
4e	–0.3021	–0.0072	8.03
4f	–0.2804	0.0035	7.73
4g	–0.2977	–0.0021	8.04
4h	–0.2770	–0.0012	7.50
4i	–0.2854	–0.0055	7.62
4j	–0.2954	–0.0010	8.01

4.3. Molecular Electrostatic Potential (MEP) Analysis

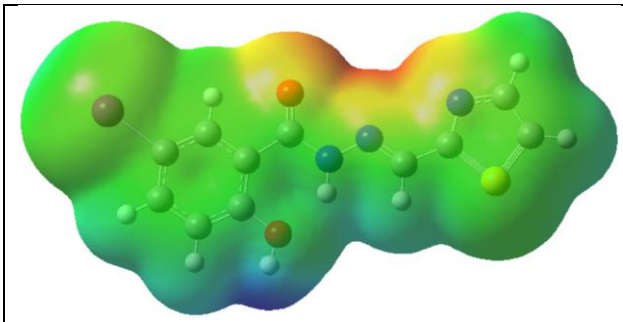

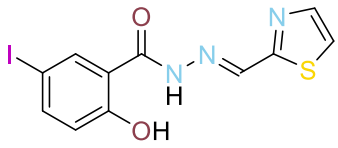

4a

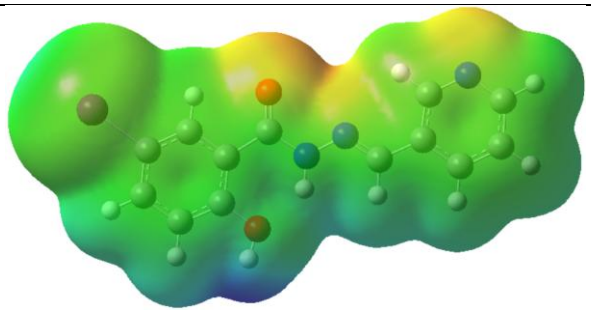

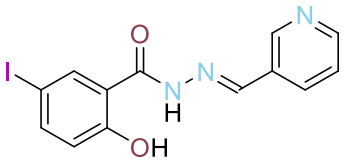

4b

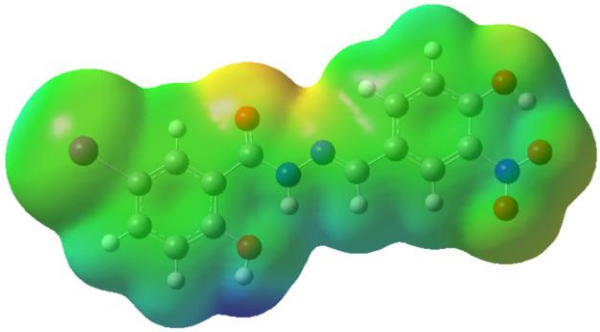

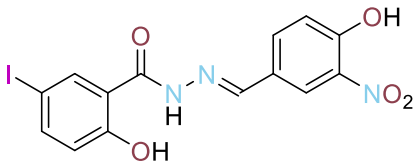

4c

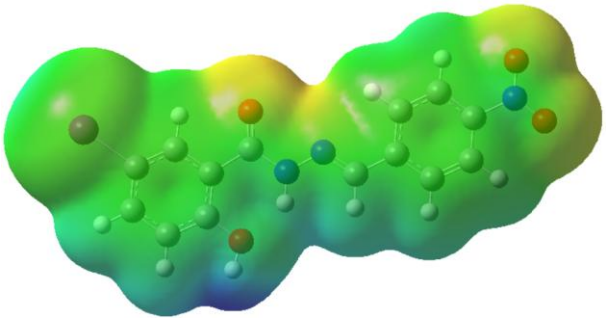

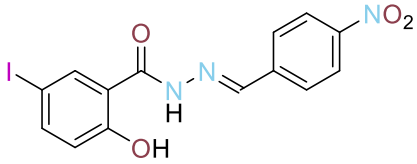

4d

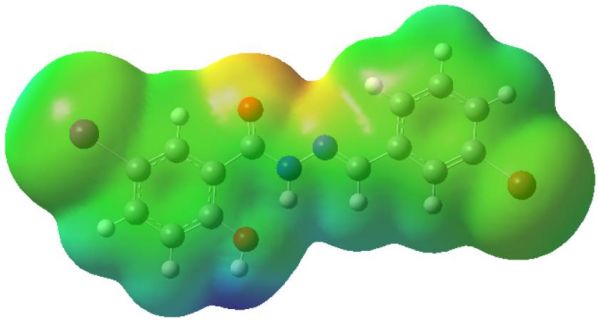

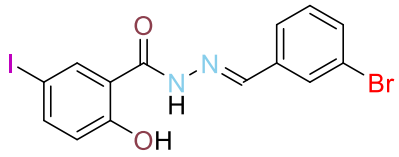

4e

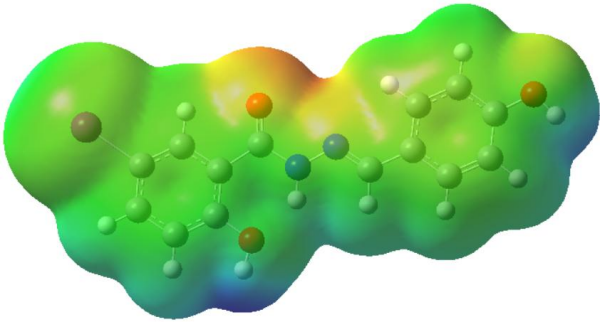

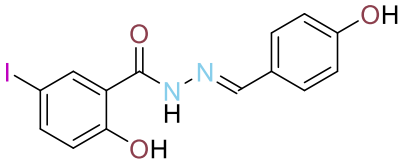

4f

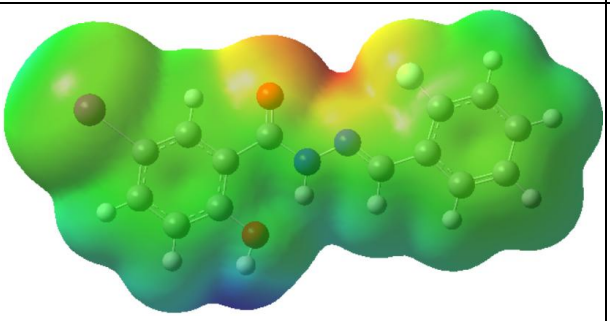

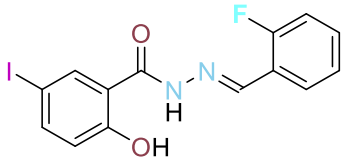

4g

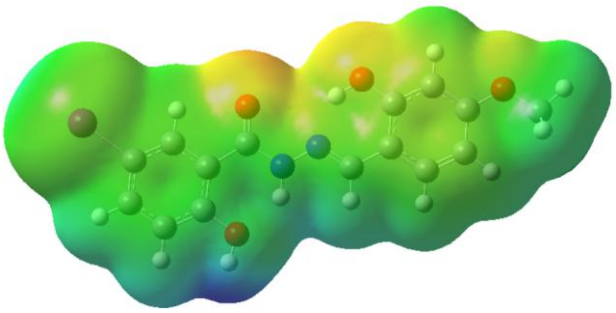

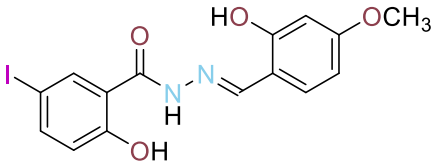

4h

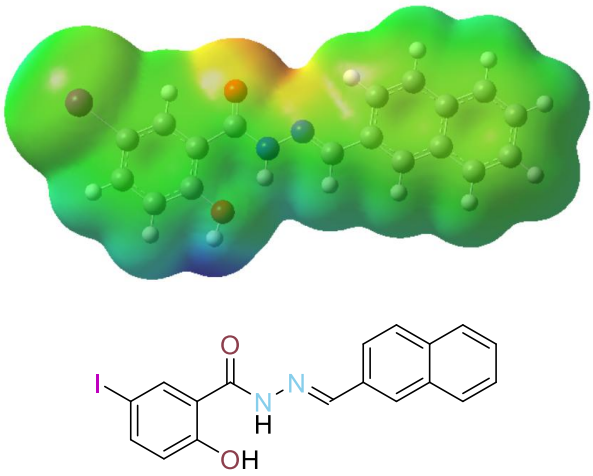

4i

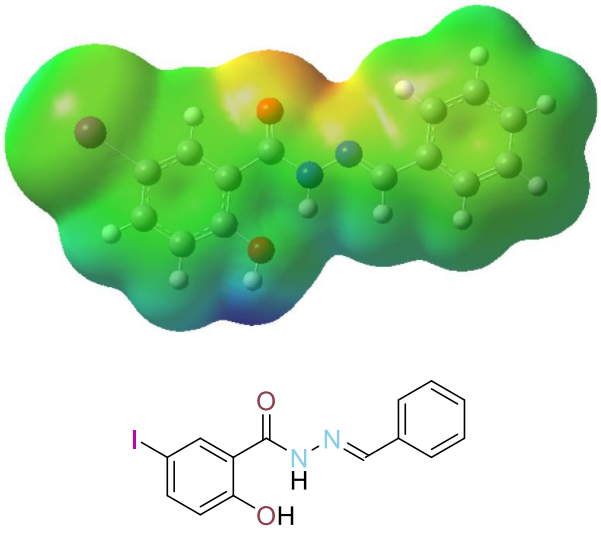

4j

Molecular electrostatic potential (MEP) maps were generated by mapping the charge distribution over the electron density. It shows the partial distribution of change along the molecule's surface. For all the compounds, the most electrophilic site is the very acidic proton of the hydroxyl group; whereas the nucleophilic site shifts or gets contribution of different parts regarding to the nature of the R group (substituent). It is partially or mostly located at the carboxylic oxygen and the imidic nitrogen.

Table S3. Cartesian coordinates (xyz) of the geometry optimizations for compounds **4a-j** calculated at the ωB97X-D/def2-tzvpp level.

4a

E(scf) = -1433.70369823 a.u.

N	1.483436	2.425561	0.000000
C	2.691685	2.834798	0.000000
H	3.547675	2.135975	0.000000
N	1.283579	1.102144	0.000000
H	2.071843	0.453774	0.000000
C	0.000000	0.592741	0.000000
O	-0.985035	1.287706	0.000000
C	-0.112017	-0.919879	0.000000
C	0.938350	-1.855910	0.000000
C	-1.427123	-1.402126	0.000000
C	0.655814	-3.224630	0.000000
C	-1.703528	-2.763385	0.000000
H	-2.220282	-0.652460	0.000000
C	-0.655051	-3.683762	0.000000
H	1.480051	-3.943760	0.000000
H	-0.850849	-4.757223	0.000000
O	2.226765	-1.425634	0.000000
H	2.830738	-2.174284	0.000000
I	-3.695812	-3.437547	0.000000
C	3.013354	4.262557	0.000000
C	2.812649	6.448824	0.000000
C	4.180380	6.394536	0.000000
H	2.232882	7.372864	0.000000
H	4.890929	7.218331	0.000000
N	2.167945	5.249642	0.000000
S	4.690588	4.756011	0.000000

4b

E(scf) = -1112.98974026 a.u.

N	0.984926	2.721415	0.000000
C	2.042758	3.433380	0.000000
H	3.051031	2.978200	0.000000
N	1.119073	1.386582	0.000000
H	2.043200	0.954505	0.000000
C	0.000000	0.582833	0.000000
O	-1.124990	1.020327	0.000000
C	0.254901	-0.911865	0.000000
C	1.500001	-1.566615	0.000000
C	-0.905089	-1.696760	0.000000
C	1.555949	-2.963062	0.000000
C	-0.845077	-3.084560	0.000000
H	-1.855223	-1.159721	0.000000
C	0.394441	-3.724850	0.000000
H	2.529283	-3.462256	0.000000
H	0.463474	-4.813858	0.000000
O	2.646154	-0.837564	0.000000
H	3.412758	-1.418550	0.000000
I	-2.615876	-4.219464	0.000000
C	1.976269	4.900203	0.000000
C	3.143635	5.667938	0.000000
C	0.747249	5.583494	0.000000
C	3.041330	7.055722	0.000000
H	4.123499	5.181707	0.000000
H	-0.181667	5.004309	0.000000
C	1.769366	7.624683	0.000000
H	3.930702	7.688129	0.000000
H	1.652046	8.713816	0.000000
N	0.645806	6.906283	0.000000

4c

E(scf) = -1376.41173575 a.u.

N	1.315769	0.859890	0.000000
C	1.689993	2.078424	0.000000
H	0.967414	2.914738	0.000000
N	0.000000	0.596590	0.000000
H	-0.684820	1.352621	0.000000
C	-0.437998	-0.709341	0.000000
O	0.313179	-1.654827	0.000000
C	-1.940784	-0.906442	0.000000
C	-2.932494	0.091573	0.000000
C	-2.350124	-2.245952	0.000000
C	-4.283758	-0.265133	0.000000
C	-3.694344	-2.596156	0.000000
H	-1.558379	-2.997010	0.000000
C	-4.670426	-1.599246	0.000000
H	-5.046889	0.518492	0.000000
H	-5.731630	-1.853254	0.000000
O	-2.572088	1.401056	0.000000
H	-3.351859	1.964363	0.000000
I	-4.259305	-4.622051	0.000000
C	3.115652	2.427828	0.000000
C	3.510425	3.755268	0.000000
C	4.114798	1.426802	0.000000
C	4.870228	4.092046	0.000000
H	2.783315	4.568160	0.000000
H	3.798137	0.381721	0.000000
C	5.875966	3.099783	0.000000
C	5.452445	1.754147	0.000000
H	6.226561	0.985599	0.000000
N	5.221143	5.499027	0.000000
O	6.416988	5.791951	0.000000
O	4.341559	6.324453	0.000000
O	7.173514	3.349590	0.000000
H	7.280216	4.325336	0.000000

4d

E(scf) = -1301.25786890 a.u.

N	-0.192089	-1.836659	0.000000
C	-0.931129	-2.876206	0.000000
H	-2.034137	-2.810855	0.000000
N	-0.777849	-0.634268	0.000000
H	-1.794446	-0.544966	0.000000
C	0.000000	0.506830	0.000000
O	1.206134	0.475838	0.000000
C	-0.749420	1.822654	0.000000
C	-2.143661	2.010082	0.000000
C	0.071651	2.957669	0.000000
C	-2.675068	3.302624	0.000000
C	-0.460598	4.240558	0.000000
H	1.148413	2.779938	0.000000
C	-1.844919	4.416144	0.000000
H	-3.760458	3.437953	0.000000
H	-2.283230	5.415428	0.000000
O	-2.969620	0.931812	0.000000
H	-3.889550	1.213181	0.000000
I	0.812985	5.913987	0.000000
C	-0.335992	-4.220134	0.000000
C	-1.168048	-5.347503	0.000000
C	1.058124	-4.391094	0.000000
C	-0.628228	-6.628921	0.000000
H	-2.253535	-5.221931	0.000000
H	1.695303	-3.505172	0.000000
C	0.754702	-6.765893	0.000000
C	1.608258	-5.664195	0.000000
H	2.686142	-5.822475	0.000000
H	-1.255362	-7.519632	0.000000
N	1.334645	-8.120218	0.000000
O	2.542344	-8.212352	0.000000
O	0.566851	-9.057854	0.000000

4e

E(scf) = -3670.27718707 a.u.

N	1.326529	0.569920	0.000000
C	1.755026	1.770580	0.000000
H	1.066337	2.635419	0.000000
N	0.000000	0.369090	0.000000
H	-0.647828	1.157118	0.000000
C	-0.500892	-0.914060	0.000000
O	0.202207	-1.895649	0.000000
C	-2.011947	-1.037740	0.000000
C	-2.954469	0.006749	0.000000
C	-2.485465	-2.355808	0.000000
C	-4.321356	-0.284604	0.000000
C	-3.844968	-2.640993	0.000000
H	-1.730397	-3.143823	0.000000
C	-4.772063	-1.598458	0.000000
H	-5.045771	0.535001	0.000000
H	-5.844281	-1.801011	0.000000
O	-2.531593	1.297374	0.000000
H	-3.283549	1.897235	0.000000
I	-4.506154	-4.637704	0.000000
C	3.196280	2.063371	0.000000
C	3.622795	3.396247	0.000000
C	4.147542	1.032858	0.000000
C	4.985175	3.686242	0.000000
H	2.892669	4.208581	0.000000
H	3.800077	-0.001692	0.000000
C	5.935033	2.667993	0.000000
C	5.502370	1.340062	0.000000
H	6.241783	0.536610	0.000000
H	6.999052	2.908616	0.000000
Br	5.548830	5.493850	0.000000

4f

E(scf) = -1172.12060312 a.u.

N	1.897464	1.612248	0.000000
C	3.168915	1.711256	0.000000
H	3.818307	0.815219	0.000000
N	1.363712	0.376281	0.000000
H	1.963465	-0.448370	0.000000
C	0.000000	0.214062	0.000000
O	-0.778749	1.138150	0.000000
C	-0.498951	-1.219802	0.000000
C	0.273997	-2.395332	0.000000
C	-1.893517	-1.346915	0.000000
C	-0.352108	-3.644978	0.000000
C	-2.511805	-2.590934	0.000000
H	-2.464951	-0.417070	0.000000
C	-1.737124	-3.750922	0.000000
H	0.258903	-4.552347	0.000000
H	-2.203276	-4.737512	0.000000
O	1.629782	-2.312580	0.000000
H	2.018612	-3.192278	0.000000
I	-4.611114	-2.728129	0.000000
C	3.841908	3.014449	0.000000
C	5.238008	3.082752	0.000000
C	3.111373	4.215600	0.000000
C	5.897408	4.309592	0.000000
H	5.826915	2.161281	0.000000
H	2.020829	4.162734	0.000000
C	5.159341	5.496327	0.000000
C	3.757905	5.439969	0.000000
H	3.197092	6.376027	0.000000
H	6.990747	4.344849	0.000000
O	5.737414	6.715213	0.000000
H	6.694505	6.621608	0.000000

4g

E(scf) = -1196.10290254 a.u.

N	1.362017	2.292838	0.000000
C	2.544626	2.771242	0.000000
H	3.428136	2.104411	0.000000
N	1.244835	0.954723	0.000000
H	2.074012	0.360121	0.000000
C	0.000000	0.366818	0.000000
O	-1.030183	0.995499	0.000000
C	-0.016247	-1.151316	0.000000
C	1.090496	-2.019951	0.000000
C	-1.298056	-1.715647	0.000000
C	0.894530	-3.403855	0.000000
C	-1.488411	-3.091701	0.000000
H	-2.136667	-1.017322	0.000000
C	-0.384799	-3.944826	0.000000
H	1.762440	-4.069683	0.000000
H	-0.512831	-5.028475	0.000000
O	2.349706	-1.510451	0.000000
H	2.998167	-2.220804	0.000000
I	-3.435031	-3.889321	0.000000
C	2.853908	4.205581	0.000000
C	4.202181	4.598629	0.000000
C	1.890323	5.227961	0.000000
C	4.578798	5.936983	0.000000
H	4.970817	3.821062	0.000000
C	3.596783	6.927095	0.000000
C	2.251031	6.570698	0.000000
H	1.457917	7.319974	0.000000
H	5.636041	6.207309	0.000000
H	3.876339	7.982500	0.000000
F	0.600791	4.932817	0.000000

4h

E(scf) = -1286.54090545 a.u.

N	-0.366237	-1.918427	0.000000
C	-1.161692	-2.922576	0.000000
H	-2.258135	-2.787323	0.000000
N	-0.866591	-0.667567	0.000000
H	-1.872679	-0.507102	0.000000
C	0.000000	0.396089	0.000000
O	1.202381	0.257333	0.000000
C	-0.627655	1.773243	0.000000
C	-2.000182	2.081070	0.000000
C	0.289317	2.831648	0.000000
C	-2.417359	3.414727	0.000000
C	-0.129863	4.156126	0.000000
H	1.346341	2.559979	0.000000
C	-1.493247	4.451998	0.000000
H	-3.486900	3.643991	0.000000
H	-1.842743	5.485695	0.000000
O	-2.915639	1.077520	0.000000
H	-3.807649	1.437451	0.000000
I	1.284585	5.712716	0.000000
C	-0.651226	-4.283185	0.000000
C	-1.538909	-5.366391	0.000000
C	0.748642	-4.552268	0.000000
C	-1.105688	-6.684089	0.000000
H	-2.613539	-5.162373	0.000000
C	0.278376	-6.936270	0.000000
C	1.187269	-5.877587	0.000000
H	2.257281	-6.084804	0.000000
H	-1.834365	-7.493123	0.000000
O	1.661516	-3.589338	0.000000
H	1.213401	-2.712327	0.000000
O	0.814239	-8.171391	0.000000
C	-0.031927	-9.288645	0.000000
H	0.616913	-10.172866	0.000000

H	-0.673103	-9.317761	0.898042
H	-0.673103	-9.317761	-0.898042

4i

E(scf) = -1250.45901065 a.u.

N	1.313909	0.994102	0.000000
C	1.665316	2.220170	0.000000
H	0.921285	3.038417	0.000000
N	0.000000	0.713389	0.000000
H	-0.692739	1.461915	0.000000
C	-0.423855	-0.595452	0.000000
O	0.334239	-1.535822	0.000000
C	-1.926044	-0.808006	0.000000
C	-2.929034	0.178631	0.000000
C	-2.321162	-2.151618	0.000000
C	-4.276376	-0.192857	0.000000
C	-3.661588	-2.516545	0.000000
H	-1.521095	-2.893815	0.000000
C	-4.648883	-1.531062	0.000000
H	-5.047939	0.582558	0.000000
H	-5.707228	-1.796769	0.000000
O	-2.583886	1.492271	0.000000
H	-3.370576	2.045696	0.000000
I	-4.203802	-4.549065	0.000000
C	3.081028	2.607897	0.000000
C	3.429664	3.941782	0.000000
C	4.103173	1.614059	0.000000
C	4.790549	4.349521	0.000000
H	2.651587	4.711205	0.000000
C	5.421526	1.979561	0.000000
H	3.803398	0.564678	0.000000
C	5.169624	5.719516	0.000000
C	5.807286	3.351641	0.000000
H	6.202172	1.214720	0.000000
C	6.495043	6.081399	0.000000

4j

E(scf) = -1096.97618261 a.u.

N	1.024269	2.699636	0.000000
C	2.098135	3.387088	0.000000
H	3.094319	2.906245	0.000000
N	1.131916	1.359948	0.000000
H	2.047734	0.911113	0.000000
C	0.000000	0.578669	0.000000
O	-1.118579	1.034696	0.000000
C	0.227087	-0.921549	0.000000
C	1.459482	-1.600034	0.000000
C	-0.947241	-1.684567	0.000000
C	1.489048	-2.997390	0.000000
C	-0.913438	-3.073303	0.000000
H	-1.886805	-1.129296	0.000000
C	0.313432	-3.737287	0.000000
H	2.452842	-3.514794	0.000000
H	0.361792	-4.827404	0.000000
O	2.619200	-0.893168	0.000000
H	3.374601	-1.488576	0.000000
I	-2.705663	-4.174581	0.000000
C	2.069318	4.856761	0.000000
C	3.272036	5.573580	0.000000
C	0.853908	5.557997	0.000000
C	3.265453	6.967141	0.000000
H	4.223208	5.033729	0.000000
C	2.054712	7.656886	0.000000
C	0.850600	6.947867	0.000000
H	-0.099489	7.486515	0.000000
H	4.209492	7.516124	0.000000
H	2.047172	8.749035	0.000000
H	-0.078152	4.989622	0.000000

H	4.387800	6.483381	0.000000
C	7.168159	3.756859	0.000000
C	7.505294	5.089431	0.000000
H	6.774416	7.137192	0.000000
H	7.946169	2.989336	0.000000
H	8.555726	5.388329	0.000000

5. Molecular Simulation Methods

5.1. Schiff base derivatives library preparation

The Schiff base Salicylic derivatives were 3D modeled in mol2 format and minimized with the molecular visualization software Maestro v 14.2 (Schrödinger LLC, NY, 2024-1) under the OPLS-AA forcefield. Additionally, the 3D structures of commercially available drug acarbose was retrieved from chEMBL database (https://www.ebi.ac.uk/chembl/explore/compound/CHEMBL1566) to act as positive control.

5.2 Molecular targets preparation

The structures of the co-crystallized enzyme-inhibitor complex of human alpha glucosidase (α-GLU) was retrieved from the RCSB Protein Data Bank database (PDB code 2QMJ).[5] The structure of α-GLU in complex to acarbose was visualized in Maestro Suite v. 14. 2 (OPLS-AA forcefield) and processed with the protein preparation workflow for the identification of the atom types, bond distances, addition of hydrogens, creation of disulfide bonds, and pH 6.8 using the *Propka* method.[6] Triplicate conventional molecular dynamics simulations (cMDs) were performed with *multisim* software v. 3.8.5.19, under the Desmond software package. The parameters and topologies describing the enzyme and the inhibitors for proteins and organic molecules were calculated with OPLS-AA forcefield.[7] The enzyme-inhibitor complexes were solvated in an orthorhombic chemical space of 15 Å buffered edge size using the SPC water model (optimized for liquid simulations) and 0.15 M NaCl. The total number of atoms of the solvated system comprised 68,681 atoms (863 amino acids, 19,244 explicit water molecules). An initial minimization stage of 50,000 steps was performed under the combined steepest descendant/conjugated gradient algorithm. A second stage of simulated annealing was performed

under NvT ensemble for the next steps: 500 ps at 10 K, 1500 ps at 100 K, 1000 ps at 300 K, 100 ps at 400 K, and finally, 2000 ps at 300 K. The system was then equilibrated for 10,500 ps with conventional molecular dynamics under NpT ensemble (pressure = 1 atm, 298 K). Long-range electrostatic interactions were calculated with the Particle Mesh Ewald method (tolerance $1x10^{-12}$), and integration times of 2 fs. Production calculations were performed for triplicate 500 ns of Conventional Molecular Dynamics Simulations. The concatenated production trajectories were subjected to Hierarchical clustering, and more populated conformations were retrieved for receptor-based molecular docking calculations.

5.3 Ensemble molecular docking calculations

From the selected conformations MDs, ten representative conformers of α-GLU target were extracted and docked with the derivative library using the GPU version of AutoDock Vina (GNINA V 1.1)[8] and the Vinardo scoring function (Monte Car-lo-Metropolis exhaustive search method of 100).[9] The chemical search space consisted of an orthorhombic system of 25 Å per side and was situated in the Cartesian coordinates of α-GLU (-17.88, 6.37, 5.41). All BFE values in Kcal/mol were corrected and classified using a neural network method, which is included in the redock_default2018 set in the GNINA program. The results were expressed as the mean of BFE (Kcal/mol) ± standard deviation of the values calculated for each conformer (n=10) and the binding mode of each derivative (n=5) in the database (GraphPad Prism, V 9.5.0 (730), USA).

Table S4: Binding Free energy and CNN-based calculated affinity in pK units obtained from molecular dynamic simulations

Compounds	BFE (Kcal mol-1)	Std.Dev	AFF (pK units)	Std.Dev
4a	-6.46	0.62	4.74	0.33
4b	-5.83	0.58	4.78	0.35
4c	-6.62	0.66	4.60	0.27
4d	-6.61	0.78	4.69	0.27
4e	-7.23	0.64	4.63	0.26
4f	-6.87	0.60	4.77	0.26
4g	-7.09	0.63	4.71	0.23
4h	-6.59	0.59	4.64	0.24
4i	-7.10	0.88	4.67	0.20
4j	-7.38	0.82	4.78	0.31
Acarbose	-7.41	0.79	5.00	0.22

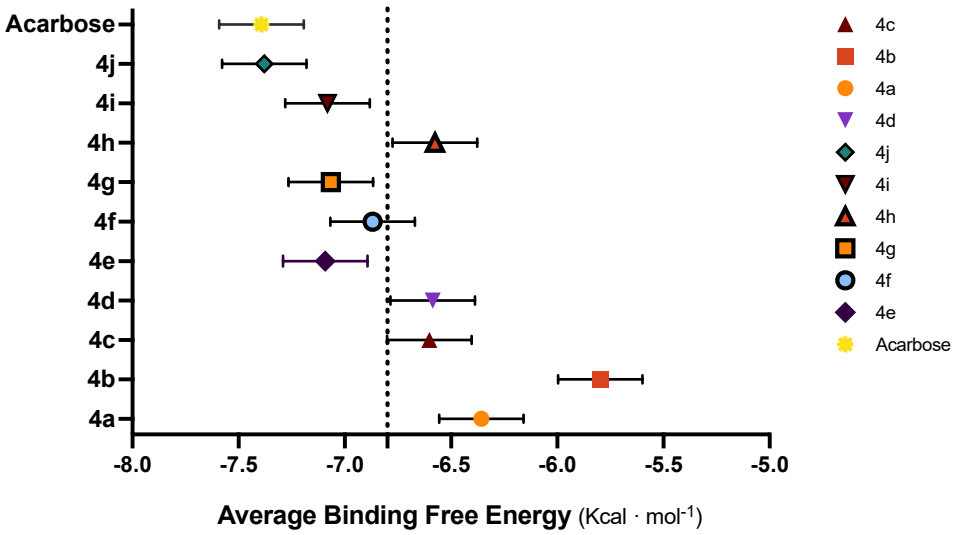

Figure S2. Calculated average binding free energies of Schiff base salicylic derivatives.

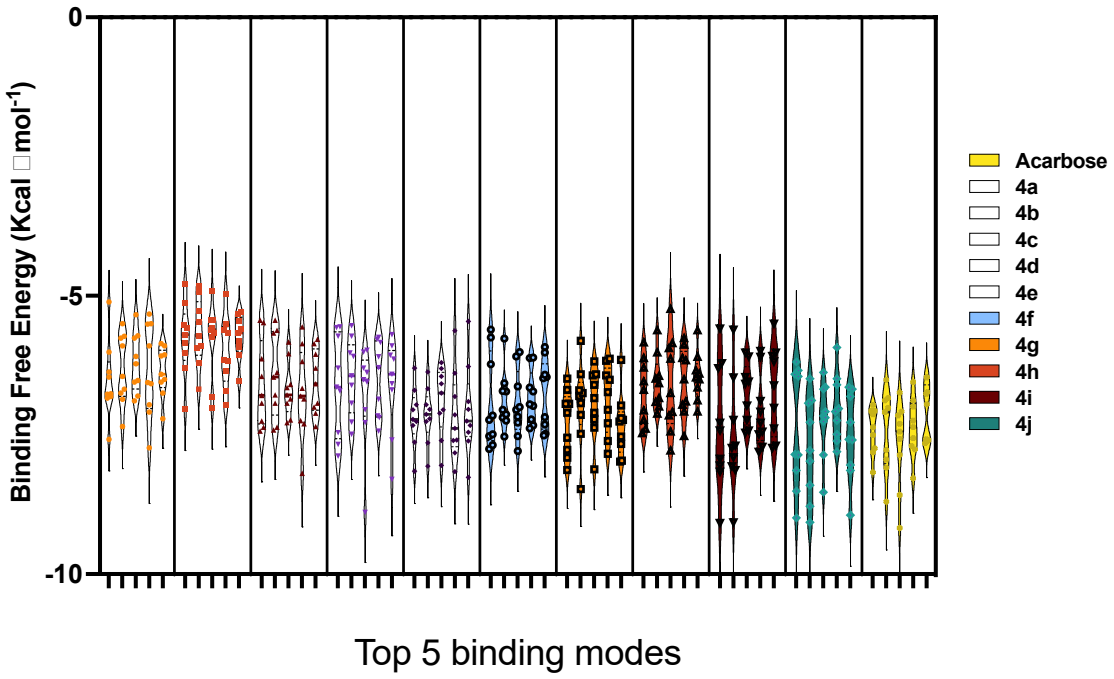

Figure S3: Violin plot of binding free energy (BFE) values for each binding mode of Schiff base derivatives **4a–4j** and the positive control Acarbose. The distribution of BFE values is shown, with markers representing individual data points. Compounds **4j**, **4i**, and **4d** demonstrate more negative BFE values, indicating stronger binding affinity, while Acarbose is included as a reference.

5.4 Molecular dynamics of selected Schiff base derivatives

Initial coordinates of the **4e** and **4j** in complex to a-GLU were retrieved from molecular docking analysis. The simulation systems comprised ca. 68,620 atoms, and all simulation steps were performed as previously described for 2QMJ at 2 fs integration time.

5.5 ADMET profiling of selected Schiff base derivatives

The ADMETLab v3.0 (https://admetlab3.scbdd.com/server/evaluationCal) was used to calculate relevant pharmacokinetic parameters of **4e** and **4j** Schiff base derivatives. SMILES structures were derived from docked mol2 of ligands, and stored as csv file.

6. Plots, Statistical Analysis and Visualizations

6.1. Descriptive Statistics

Metrics: Mean, Standard Deviation (SD), and Coefficient of Variation

Table S5: Descriptive statistics

Compounds	A 450 nm			% inhibition			Mean	SD	CV
	R1	R2	R3	R1	R2	R3			
4a	0.723	0.809	0.809	71.835	61.384	66.926	66.715	4.269	6.399
4b	1.086	1.128	1.196	57.694	46.158	51.104	51.652	4.726	9.149
4c	1.166	1.334	1.33	54.577	36.325	45.626	45.509	7.452	16.375
4d	0.945	0.847	1.056	63.187	59.570	56.827	59.861	2.604	4.350
4e	0.11	0.217	0.203	95.715	89.642	91.701	92.353	2.522	2.731
4f	1.067	0.959	1.111	58.434	54.224	54.579	55.746	1.906	3.420
4g	0.329	0.346	0.333	87.183	83.484	86.386	85.685	1.589	1.855
4h	2.025	2.013	2.007	21.114	3.914	17.948	14.325	7.474	52.177
4i	0.265	0.256	0.282	89.677	87.780	88.471	88.643	0.784	0.884
4j	0.13	0.108	0.202	94.936	94.845	91.742	93.841	1.485	1.582
Acarbose	0.399	0.337	0.352	84.457	83.914	85.609	84.660	0.707	0.835
Buffer	2.567	2.095	2.446						

During the evaluation of % inhibition, compound **4j** demonstrated the highest inhibitory activity with a mean % inhibition of 93.84% (R1 = 94.94%, R2 = 94.85%, R3 = 91.74%) and minimal variability (SD = 1.485, CV = 1.582%), indicating excellent reproducibility. Compound **4e** also displayed potent inhibitory activity, with a mean % inhibition of 92.35% (R1 = 95.72%, R2 = 89.64%, R3 = 91.70%) and low variability (SD = 2.522, CV = 2.731%).

Compound **4i** demonstrated a mean % inhibition of 88.64% (R1 = 89.68%, R2 = 87.78%, R3 = 88.47%) with exceptional reproducibility (SD = 0.784, CV = 0.884%). Despite its strong inhibitory activity, compound **4g** also exhibited promising results with a mean % inhibition of 85.69% (R1 = 87.18%, R2 = 83.48%, R3 = 86.38%) and low variability (SD = 1.589, CV = 1.855%). The

activity of these compounds exceeded the positive control, **Acarbose**, which showed a mean % inhibition of 84.66% (SD = 0.707, CV = 0.835%).

Notably, compound **4h** displayed minimal activity, with a mean % inhibition of 14.33% and a high CV of 52.177%, indicating variability across replicates. Other compounds, such as **4a, 4b, 4c,** and **4f**, showed moderate inhibitory activity ranging from 45.51% to 66.71%, but their performance was less consistent compared to the top-performing compounds.

Compounds **4e, 4j, 4i,** and **4g** emerge as the most promising candidates for further investigation due to their potent activity and reproducibility. Unlike **4i**, which showed solubility issues during subsequent evaluations such as IC50 determination and enzyme kinetics, **4e** and **4j** did not exhibit solubility limitations and were successfully subjected to extended experimental analyses. Their robust performance, coupled with strong inhibitory activity, positions them as lead candidates for in-depth structure-activity relationship (SAR) analysis, molecular docking, and IC50 determination.

The case of **4i** highlights the critical balance between biological activity and physicochemical properties, such as solubility, in drug development. Strategies such as prodrug formation, the use of solubilizing agents, or structural modifications may be explored to improve its solubility and unlock its potential as a highly potent α-glucosidase inhibitor.

6.2. Comparative Analysis

A. Comparison of Compounds

1) ANOVA Results:

F-statistic: 77.40

p-value: 8.85×10^{-15}

Since the **p-value** is extremely small (**$p < 0.05$**), there are statistically significant differences in % inhibition among the compounds.

2) Tukey's Post-hoc Test Results

Tukey's post-hoc test was performed to identify specific pairs of compounds that exhibited statistically significant differences in % inhibition following a significant result from the one-way ANOVA test.

Table S6: Tukey's post-hoc test results

group1	group2	meandiff	p-adj	lower	upper	reject
4a	**4b**	-15.063	0.0322	-29.3043	-0.8217	TRUE
4a	**4c**	-21.2057	0.001	-35.447	-6.9643	TRUE
4a	**4d**	-6.8537	0.8103	-21.095	7.3877	FALSE
4a	**4e**	25.6377	0.0001	11.3963	39.879	TRUE
4a	**4f**	-10.9693	0.239	-25.2107	3.272	FALSE
4a	**4g**	18.9693	0.0036	4.728	33.2107	TRUE
4a	**4h**	-52.3897	0	-66.631	-38.1483	TRUE
4a	**4i**	21.9277	0.0006	7.6863	36.169	TRUE
4a	**4j**	27.126	0	12.8847	41.3673	TRUE
4a	Acarbose	17.945	0.0064	3.7037	32.1863	TRUE
4b	**4c**	-6.1427	0.8896	-20.384	8.0987	FALSE
4b	**4d**	8.2093	0.6134	-6.032	22.4507	FALSE
4b	**4e**	40.7007	0	26.4593	54.942	TRUE
4b	**4f**	4.0937	0.992	-10.1477	18.335	FALSE
4b	**4g**	34.0323	0	19.791	48.2737	TRUE

group1	group2	meandiff	p-adj	lower	upper	reject
4b	**4h**	-37.3267	0	-51.568	-23.0853	TRUE
4b	**4i**	36.9907	0	22.7493	51.232	TRUE
4b	**4j**	42.189	0	27.9477	56.4303	TRUE
4b	Acarbose	33.008	0	18.7667	47.2493	TRUE
4c	**4d**	14.352	0.0472	0.1107	28.5933	TRUE
4c	**4e**	46.8433	0	32.602	61.0847	TRUE
4c	**4f**	10.2363	0.3204	-4.005	24.4777	FALSE
4c	**4g**	40.175	0	25.9337	54.4163	TRUE
4c	**4h**	-31.184	0	-45.4253	-16.9427	TRUE
4c	**4i**	43.1333	0	28.892	57.3747	TRUE
4c	**4j**	48.3317	0	34.0903	62.573	TRUE
4c	Acarbose	39.1507	0	24.9093	53.392	TRUE
4d	**4e**	32.4913	0	18.25	46.7327	TRUE
4d	**4f**	-4.1157	0.9917	-18.357	10.1257	FALSE
4d	**4g**	25.823	0.0001	11.5817	40.0643	TRUE
4d	**4h**	-45.536	0	-59.7773	-31.2947	TRUE
4d	**4i**	28.7813	0	14.54	43.0227	TRUE
4d	**4j**	33.9797	0	19.7383	48.221	TRUE
4d	Acarbose	24.7987	0.0001	10.5573	39.04	TRUE
4e	**4f**	-36.607	0	-50.8483	-22.3657	TRUE
4e	**4g**	-6.6683	0.8331	-20.9097	7.573	FALSE
4e	**4h**	-78.0273	0	-92.2687	-63.786	TRUE
4e	**4i**	-3.71	0.9962	-17.9513	10.5313	FALSE
4e	**4j**	1.4883	1	-12.753	15.7297	FALSE
4e	Acarbose	-7.6927	0.6928	-21.934	6.5487	FALSE
4f	**4g**	29.9387	0	15.6973	44.18	TRUE
4f	**4h**	-41.4203	0	-55.6617	-27.179	TRUE
4f	**4i**	32.897	0	18.6557	47.1383	TRUE
4f	**4j**	38.0953	0	23.854	52.3367	TRUE
4f	Acarbose	28.9143	0	14.673	43.1557	TRUE
4g	**4h**	-71.359	0	-85.6003	-57.1177	TRUE
4g	**4i**	2.9583	0.9994	-11.283	17.1997	FALSE
4g	**4j**	8.1567	0.6216	-6.0847	22.398	FALSE
4g	Acarbose	-1.0243	1	-15.2657	13.217	FALSE
4h	**4i**	74.3173	0	60.076	88.5587	TRUE
4h	**4j**	79.5157	0	65.2743	93.757	TRUE
4h	Acarbose	70.3347	0	56.0933	84.576	TRUE
4i	**4j**	5.1983	0.9582	-9.043	19.4397	FALSE
4i	Acarbose	-3.9827	0.9935	-18.224	10.2587	FALSE
4j	Acarbose	-9.181	0.4639	-23.4223	5.0603	FALSE

Tukey's Post-hoc test revealed significant differences in the percentage inhibition among several compounds, highlighting their varying levels of potency. Compound **4a** demonstrated significantly higher inhibitory activity compared to **4b** and **4c**, with mean differences of -15.063 ($p = 0.0322$) and -21.206 ($p = 0.0010$), respectively. However, its performance was significantly lower than that of **4e**, which exhibited the highest inhibitory activity among all compounds tested, with a mean difference of 25.638 ($p < 0.0001$). This positions **4e** as the most potent inhibitor in this study.

Despite **4a** showing promising results, no significant differences were observed in its activity when compared to **4d** and **4f**, indicating comparable potency among these compounds. Notably, **4e**, along with **4i** and **4j**, displayed inhibitory activity comparable to or exceeding that of the reference standard, Acarbose, further emphasizing their potential as viable alternatives or improvements over existing inhibitors.

Compounds **4b**, **4c**, and **4h** demonstrated significantly lower inhibitory activity than the top-performing compounds, such as **4e** and **4j**, suggesting that these compounds may require structural optimization to enhance their efficacy. The substantial variability in the performance of **4h** (as reflected in its high coefficient of variation) underscores the need for further investigation into its stability and reliability as an inhibitor.

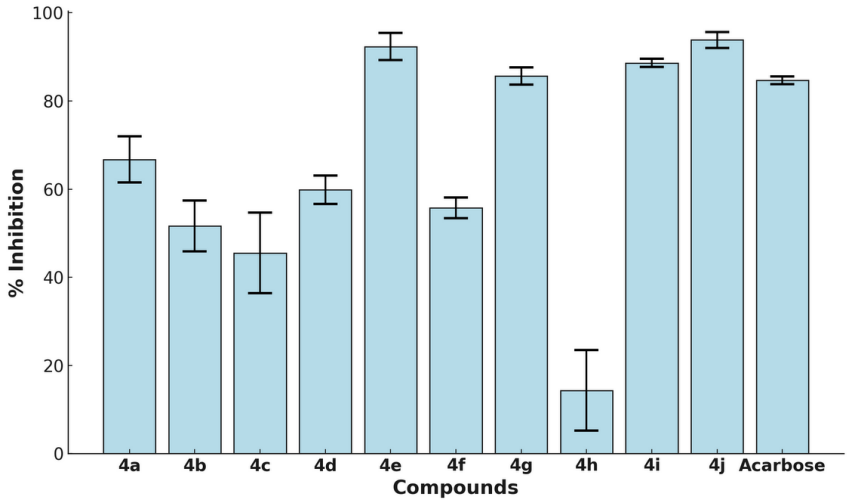

Figure S4: Bar graph representing the mean % inhibition of α-glucosidase activity for all tested compounds (**4a–4j**) and the positive control, Acarbose with error bars showing the standard deviation (SD) across three replicates.

B. Comparison to Positive Control (Acarbose)

1) Unpaired t-Tests Results:

Unpaired t-tests were performed to compare the % inhibition of the selected compounds (**4e, 4g, 4i, 4j**) against the positive control (**Acarbose**). The findings are as follows:

Compound 4e vs Acarbose:

t-statistic: 4.15

p-value: 0.041

The difference in % inhibition between compound 4e and Acarbose is statistically significant (**$p < 0.05$**). This indicates that **4e** demonstrates a significantly higher inhibitory activity compared to Acarbose.

Compound 4g vs Acarbose:

t-statistic: 0.83

p-value: 0.471

The difference in % inhibition between compound 4g and Acarbose is not statistically significant (**$p > 0.05$**). This suggests that the inhibitory activity of **4g** is comparable to Acarbose.

Compound 4i vs Acarbose:

t-statistic: 5.34

p-value: 0.006

A statistically significant difference (**$p < 0.01$**) was observed, with **4i** exhibiting superior inhibitory activity compared to Acarbose.

Compound 4j vs Acarbose:

t-statistic: 7.90

p-value: 0.005

Compound **4j** also demonstrated significantly higher inhibitory activity than Acarbose, with a highly significant difference (**$p < 0.01$**).

Compounds **4e**, **4i**, and **4j** show statistically significant improvements in inhibitory activity compared to Acarbose, with **4j** emerging as the most potent inhibitor. Compound **4g**, however, displays comparable activity to Acarbose without a statistically significant difference. These results highlight **4e**, **4i**, and **4j** as strong candidates for further investigation and potential development as α-glucosidase inhibitors.

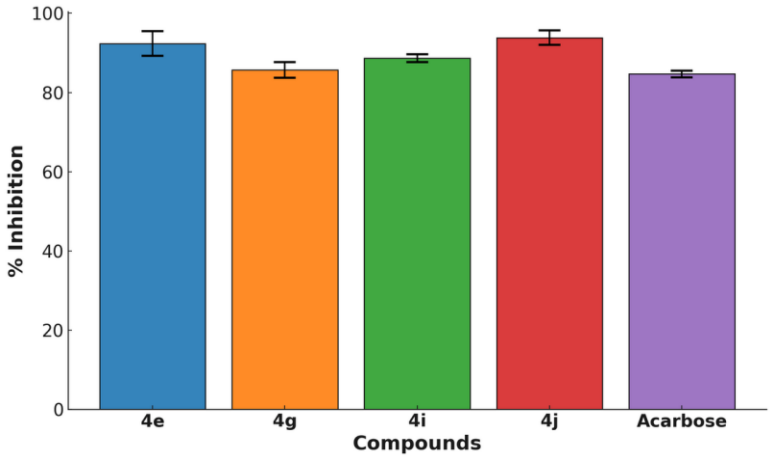

Figure S5: Bar graph comparing the % inhibition of the most active compounds (**4e**, **4g**, **4i**, and **4j**) with the positive control, Acarbose.

6.3. Variability and Reliability

1) Intra-Class Correlation Coefficient (ICC).

F-statistic: 0.451

p-value: 0.641

The p-value (0.641) is **not significant**, suggesting there is **no significant variability** between the replicates (R1, R2, R3) for % inhibition across all compounds.

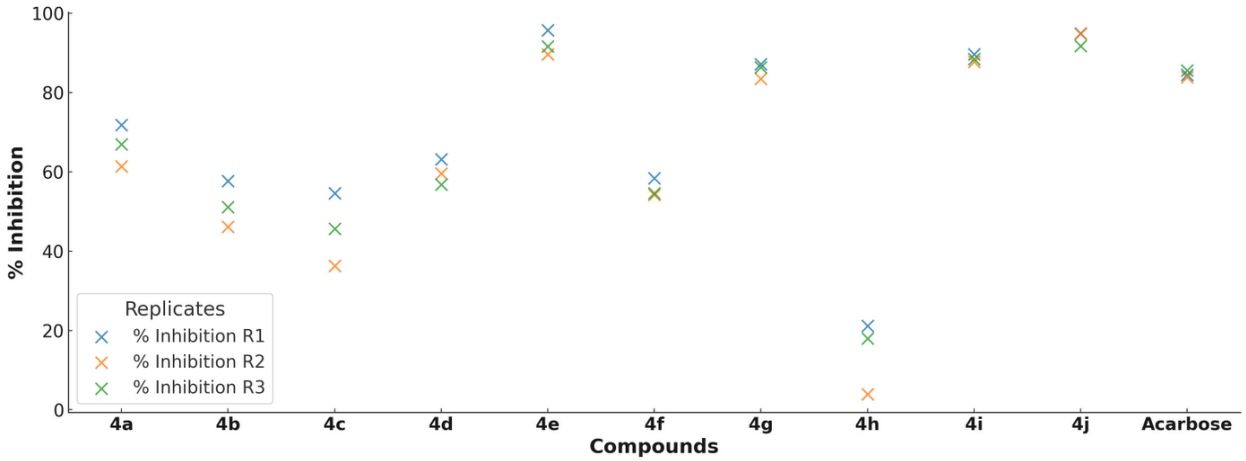

Figure S6: Scatter plot showing the % inhibition values for replicates (R1, R2, R3) across all tested compounds.

7. Structure-Activity Relationship (SAR)

7.1. Comparative % Inhibition of Compounds

The activity threshold was set at % inhibition > 84% to include Acarbose (84.66%), the standard control, as a benchmark for evaluating the inhibitory performance of the tested compounds.

Figure S7 presents the comparative % inhibition of all tested compounds, with active compounds (% inhibition > 84%) highlighted in red. The active compounds include **4i** (88.64%), **4j** (93.84%), **4e** (92.35%), **4g** (85.69%), and the standard control **Acarbose** (84.66%). These results demonstrate that compounds containing planar aromatic rings, such as naphthalene (**4i**) and benzylidene (**4j**), exhibit the highest inhibition. The planar structures likely facilitate π-π stacking interactions with the target, enhancing binding efficiency.

In addition, compounds containing electron-withdrawing halogen substituents, such as **3-Br** (**4e**) and **2-F** (**4g**), show high inhibitory activity. The electron-withdrawing nature of these substituents may optimize the electronic distribution of the molecule, improving target interaction through enhanced electronic stabilization or hydrophobic effects.

In contrast, compounds containing hydroxyl and nitro substituents, such as **4c** (4-OH, 3-NO_2), **4d** (4-NO_2), and **4h** (2-OH, 4-OCH_3), demonstrate significantly lower inhibition. These groups may introduce steric hindrance near the binding site or interfere with the molecule's electronic distribution, thereby reducing binding affinity.

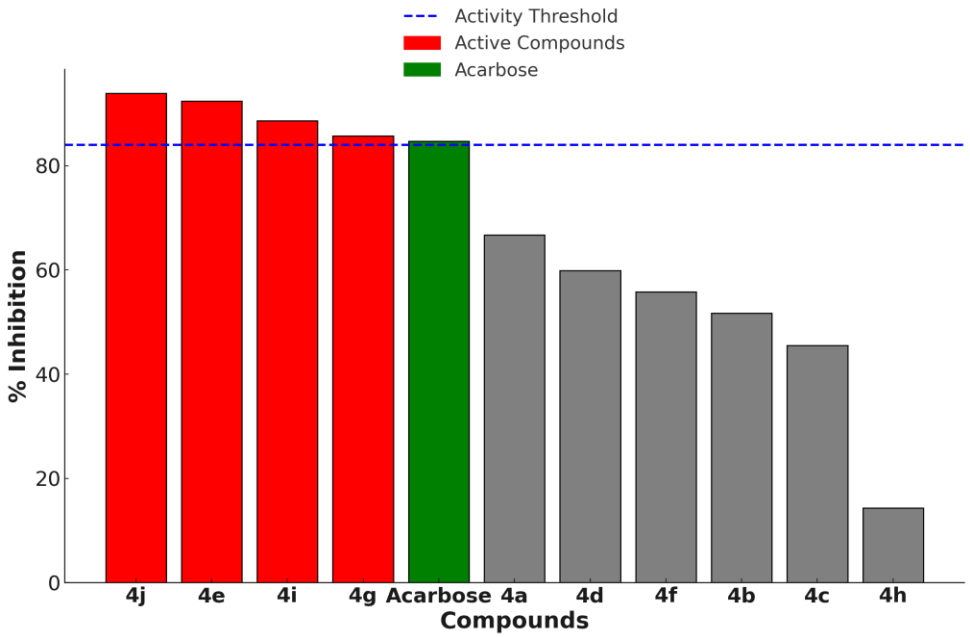

Figure S7: Comparative % inhibition of tested compounds. Active compounds (% inhibition > 84%) are highlighted in red, with the activity threshold marked as a dashed blue line.

The structure-activity relationship analysis summarized in Table S7 highlights the critical role of specific functional groups in determining the inhibitory activity of the tested compounds. Compounds with planar aromatic rings, such as **4i** (Naphthalene) and **4j** (Benzylidene), demonstrate strong inhibitory activity (% inhibition of 88.64% and 93.84%, respectively). These planar structures likely enhance binding efficiency through π–π stacking interactions with the active site of the enzyme, facilitating a stronger and more stable interaction.

Additionally, the presence of electron-withdrawing halogen groups, such as **3-Br** in **4e** (92.35% inhibition) and **2-F** in **4g** (85.69% inhibition), appears to optimize the electronic distribution within the molecule. This electronic effect enhances target interactions through improved stabilization and hydrophobic effects, contributing to higher inhibitory activity.

In contrast, **Acarbose**, the standard inhibitor, serves as a benchmark with % inhibition of 84.66%. While comparable to the active compounds, its activity is slightly lower, underscoring the superior design of the tested compounds with specific functional group modifications.

Table S7: Summary of functional groups and % inhibition of active compounds. Planar aromatic rings and electron-withdrawing halogen groups are key contributors to higher activity.

Compound	% Inhibition	Functional Group	Comments
4e	92.35	3-Bromobenzylidene	Contains electron-withdrawing 3-Br, enhancing activity
4g	85.689	2-Fluorobenzylidene	Contains electron-withdrawing 2-F, enhancing activity
4i	88.64	Naphthalene	Planar aromatic system facilitates π-π stacking
4j	93.84	Benzylidene	Planar aromatic system facilitates π-π stacking
Acarbose	84.66	Standard	Positive control for comparison.

7.2. Molecular Weight vs % Inhibition

Results:

Correlation Coefficient: -0.052

p-value: 0.886

The relationship between molecular weight and % inhibition was analyzed for all tested compounds. The correlation analysis yielded a correlation coefficient of **-0.052** and a p-value of **0.886**, indicating that the correlation is weak and not statistically significant ($p > 0.05$). Figure S8 illustrates this relationship, with active compounds (% inhibition > 84%) highlighted as red points, while less active compounds are represented as gray points. The regression line and the wide confidence interval further confirm the absence of a significant correlation.

These findings suggest a negligible inverse relationship between molecular weight and % inhibition. Notably, the active compounds are distributed across a broad range of molecular weights, reinforcing that molecular weight alone does not significantly influence inhibitory activity. Instead, functional groups, electronic effects, and molecular planarity are more critical in determining activity.

Furthermore, considerable variability in % inhibition is observed within compounds of similar molecular weights, underscoring the minimal role of molecular weight in modulating biological activity. This variability highlights the importance of designing molecules with optimized structural and electronic features for enhanced inhibitory performance.

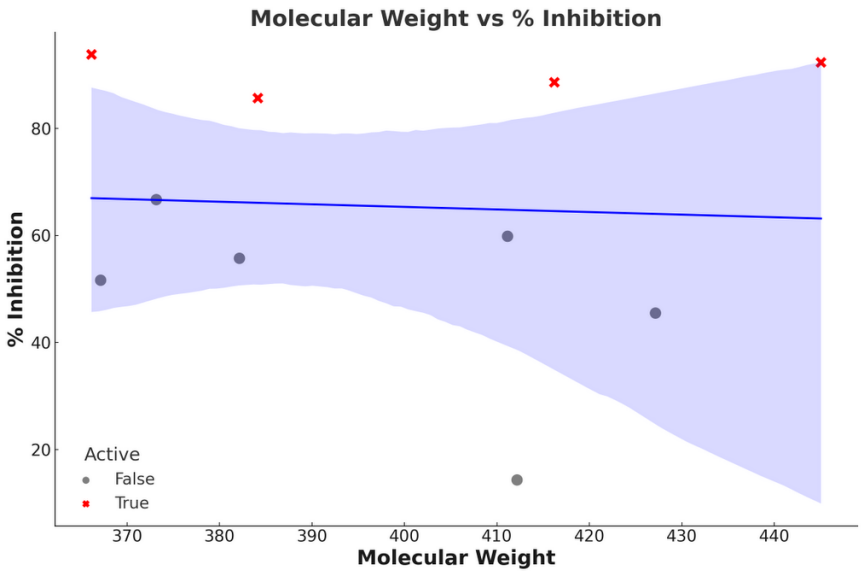

Figure S8: Scatter plot of molecular weight vs % inhibition. Active compounds (% inhibition > 84%) are highlighted in red, showing their distribution across a range of molecular weights.

7.3. Functional Groups and Their Electronic Effects Analysis:

Table S8 provides a detailed summary of the functional groups, electronic effects, and observed activity for all tested compounds. The analysis highlights the critical role of electronic effects and resonance stabilization in determining inhibitory activity.

Electron-Withdrawing Groups (EWGs): Compounds containing moderate EWGs, such as halogens, exhibit high activity. For example, **4e** (3-Br, 92.35%) and **4g** (2-F, 85.69%) demonstrate enhanced target interactions due to optimized electronic effects. The moderate electron-withdrawing effects likely facilitate favorable interactions at the binding site without causing saturation or interference. Conversely, compounds with strong EWGs, such as **4d** (4-NO_2, 59.86%), show moderate activity, possibly due to excessive electronic effects disrupting optimal binding or causing steric interference.

Electron-Donating Groups (EDGs): Compounds containing EDGs, such as OH and OCH_3 groups, exhibit reduced activity. For instance, **4f** (4-OH, 55.75%) and **4h** (2-OH, 4-OCH_3, 14.33%) display significantly lower inhibition, likely due to steric hindrance or altered electronic distribution diminishing their binding affinity. Notably, **4h**, which contains both OH and OCH_3 groups, demonstrates the lowest activity among the tested compounds.

Resonance Stabilization: The highest activity is observed for compounds with planar, resonance-stabilized aromatic systems, such as **4i** (Naphthalene, 88.64%) and **4j** (Benzylidene, 93.84%). These systems enhance inhibitory potential by facilitating π-π stacking interactions and improving electronic stabilization, thereby strengthening binding efficiency.

Table S8: Summary of functional groups, electronic effects, and their impact on % inhibition. Moderate EWG groups (halogens) and resonance stabilization are key contributors to high activity.

Compound	Functional Group	Electronic Effect	Observation
4a	Thiazole	EWG	Moderate activity (66.72%)
4b	Pyridine	EWG	Moderate activity (51.65%)
4c	4-OH, 3-NO_2	Strong EWG (NO_2), EDG (OH)	Low activity (45.51%)
4d	4-NO_2	Strong EWG	Moderate activity (59.86%)
4e	3-Br	Moderate EWG (Halogen)	High activity (92.35%)
4f	4-OH	EDG	Low activity (55.75%)
4g	2-F	Moderate EWG (Fluorine)	High activity (85.69%)
4h	2-OH, 4-OCH_3	EDG (OH, OCH_3)	Very low activity (14.33%)
4i	Naphthalene	Resonance Stabilization	Highest activity (88.64%)
4j	Benzylidene	Resonance Stabilization	High activity (93.84%)

7.4. Impact of Electronic Effects on % Inhibition

Figure S9 illustrates the relationship between electronic effects and % inhibition, categorizing compounds into groups based on their electronic properties: resonance-stabilized, electron-withdrawing groups (EWG), electron-donating groups (EDG), and mixed EWG/EDG.

Resonance-Stabilized Compounds: Resonance stabilization emerged as the most influential factor, with compounds **4i** (naphthalene, 88.64%) and **4j** (benzylidene, 93.84%) exhibiting the highest % inhibition and minimal variability. These results confirm the superior performance of planar, conjugated aromatic systems, likely due to enhanced π-π stacking interactions and improved electronic stabilization, which facilitate stronger binding to the target site.

Compounds with EWGs: Compounds containing moderate electron-withdrawing groups, such as halogens, demonstrate moderate to high activity. For example, **4e** (3-Br, 92.35%) and **4g** (2-F, 85.69%) exhibit enhanced target interactions due to their favorable electronic effects. However, the variability within this category suggests that the nature and positioning of EWGs influence

their contribution to inhibitory activity. In contrast, compounds with strong EWGs, such as **4d** (4-NO_2, 59.86%), exhibit only moderate activity, potentially due to saturation or interference with binding.

Compounds with EDGs: Electron-donating groups, such as OH and OCH_3, are associated with lower activity and higher variability. For instance, **4c** (4-OH, 3-NO_2, 45.51%), **4f** (4-OH, 55.75%), and **4h** (2-OH, 4-OCH_3, 14.33%) demonstrate reduced activity. These groups may introduce steric hindrance or disrupt the molecule's electronic distribution, limiting their ability to enhance binding.

Mixed EWG/EDG Compounds: The mixed electronic effects observed in **4c** (4-OH, 3-NO_2) result in intermediate activity. The strong EWG effect of NO_2 may partially enhance activity, but the presence of the ED OH group likely counteracts this benefit, resulting in reduced overall inhibition.

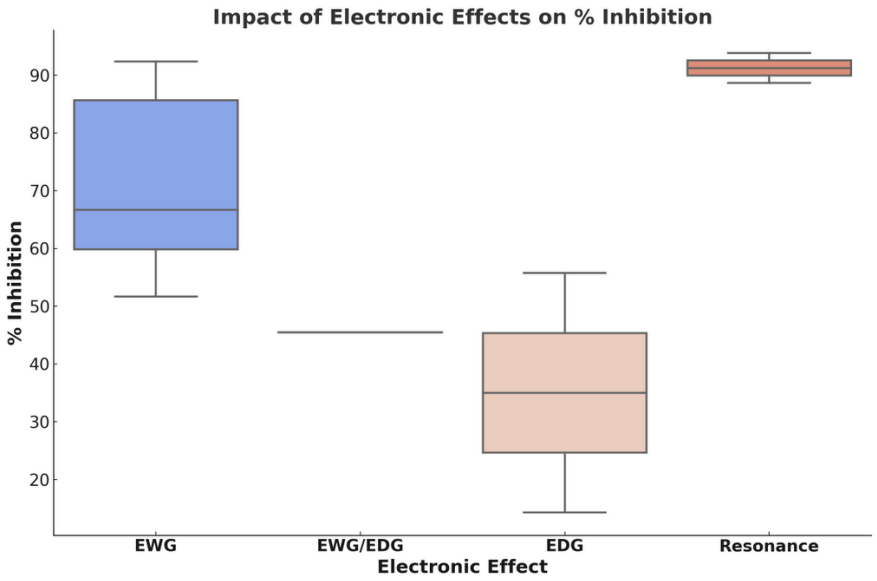

Figure S9: Impact of electronic effects on % inhibition. Resonance-stabilized compounds show the highest activity, while EWGs and EDGs exhibit variable and reduced effects, respectively.

7.5. Structure-Activity Relationship (SAR) Trends of Active Compounds

The active compounds (% inhibition > 84%) include **4i** (naphthalene), **4j** (benzylidene), **4e** (3-bromobenzylidene), **4g** (2-fluorobenzylidene), and **Acarbose**. By analyzing their functional groups, electronic effects, and structural properties, the following SAR trends are observed:

Resonance Effects Enhance Activity: Compounds **4i** and **4j**, containing resonance-stabilized aromatic systems (naphthalene and benzylidene, respectively), exhibit the highest % inhibition values. The planar and conjugated nature of these systems likely facilitates π-π stacking interactions, improving binding affinity to the target site.

Halogen Substitution Improves Activity: Halogen-substituted compounds **4e** (3-Br, 92.35%) and **4g** (2-F, 85.69%) demonstrate high inhibitory activity. The electron-withdrawing effects of bromine and fluorine enhance electronic distribution and may also improve hydrophobic interactions with the active site, contributing to their effectiveness.

Functional Group Positioning: The substitution patterns on the benzylidene group influence activity. For example, **3-Br** (4e) and **2-F** (4g) contribute to high inhibition, emphasizing the importance of functional group placement in fine-tuning activity.

Comparison to Standard (Acarbose): All active compounds either match or exceed the inhibitory activity of **Acarbose** (84.66%), a standard control, highlighting their potential as promising inhibitors.

The observed trends indicate that compounds with resonance-stabilized aromatic systems (**4i, 4j**) and electron-withdrawing halogen groups (**4e, 4g**) achieve the highest inhibitory activity. Furthermore, the absence of electron-donating groups (e.g., OH or OCH_3) correlates with higher activity, aligning with prior observations.

Table S9: SAR trends among active compounds, summarizing the relationship between functional groups, electronic effects, and % inhibition. Compounds with resonance stabilization and electron-withdrawing halogen groups demonstrate superior inhibitory potential.

Compound	% Inhibition	Functional Group	Electronic Effect	Key Trends
4i	88.64	Naphthalene	Resonance	Planar aromatic group, π-π stacking.
4j	93.84	Benzylidene	Resonance	Resonance stabilization.
4e	92.35	3-Bromobenzylidene	EWG	Halogen (Br) enhances activity.
4g	85.69	2-Fluorobenzylidene	EWG	Halogen (F) enhances activity.
Acarbose	84.66	Standard	-	Positive control

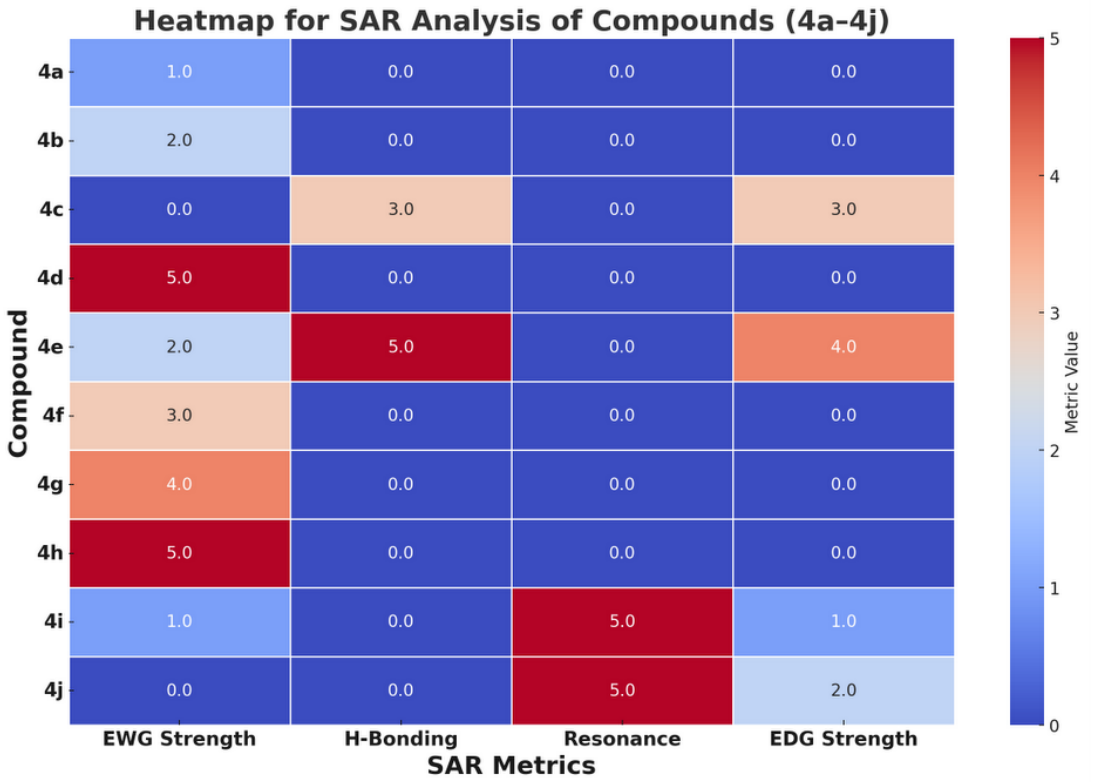

Figure S10: Heatmap illustrating the SAR metrics for compounds (**4a–4j**), including EWG strength, EDG strength, H-bonding, and resonance stabilization.

7.6. Steric Effects on % Inhibition:

Steric hindrance arises from bulky groups near the active site or key regions of the molecule, influencing binding efficiency and biological activity. Analyzing the size and positioning of substituents in both active and less active compounds highlights significant trends in steric effects. Table S10 summarizes the steric bulk and % inhibition for selected compounds. Compounds **4i** (naphthalene) and **4j** (benzylidene) exhibit planar structures, which allow for optimal π-π stacking interactions despite high steric bulk. This planarity facilitates efficient target binding, leading to the highest activity (88.64% and 93.84%, respectively).

Table S10: Steric bulk, functional groups, and % inhibition for selected compounds, illustrating the impact of steric effects on activity.

Compound	Functional Group	Steric Bulk	Observation
4j	Benzylidene	Moderate bulk, planar	**High activity (93.84%):** Planarity reduces steric hindrance.
4e	3-Bromobenzylidene	Moderate steric bulk (Br)	**High activity (92.35%):** Halogen size is moderate, favorable for binding.
4i	Naphthalene	High steric bulk, planar	**High activity (88.64%):** Planar naphthalene allows π-π stacking despite bulk.
4g	2-Fluorobenzylidene	Small bulk (F)	**High activity (85.69%):** Small size of fluorine reduces steric clash.
4c	4-OH, 3-NO_2	Bulky NO_2 and OH groups	**Low activity (45.51%):** Steric clashes and electronic effects reduce activity.
4h	2-OH, 4-OCH_3	Moderate steric hindrance	**Low activity (14.33%):** Bulky methoxy group near active site reduces binding.

Moderate steric bulk, such as the halogen substituents in **4e** (3-Br) and **4g** (2-F), is well-tolerated and maintains high activity. The moderate size of halogens like Br and F balances their electronic effects with minimal steric hindrance, contributing to strong inhibitory performance (92.35% and 85.69%, respectively).

In contrast, compounds with bulky substituents, such as OCH_3 and NO_2 (**4h** and **4c**), display significantly lower activity (14.33% and 45.51%). These groups likely introduce steric clashes or disrupt the optimal orientation of the molecule at the active site, reducing binding efficiency.

Steric Hindrance: Compounds with moderate steric hindrance achieve the highest % inhibition, whereas high steric hindrance reduces activity due to unfavorable interactions or disrupted binding orientation. For example, compounds **4e** and **4g**, which contain moderately sized halogen substituents, exhibit strong inhibitory activity, while bulky groups such as OCH_3 and NO_2 in **4h** and **4c** lead to poor performance.

Planarity: Planar compounds, such as **4i** and **4j**, demonstrate consistently high activity with minimal variability, confirming the importance of molecular planarity for efficient π-π stacking interactions at the target site. Non-planar compounds exhibit a broader range of activity, including significantly lower values, highlighting the importance of structural alignment for biological performance.

Comparison of Planar vs. Bulky Groups: A comparison of planar and bulky compounds reveals that planar structures consistently outperform bulky groups in % inhibition. Planar compounds, such as **4i** and **4j**, achieve an average inhibition of ~91.24% with lower variability, while compounds with significant steric bulk display reduced and more variable activity (mean ~59.87%). These results reinforce the disruptive impact of steric hindrance on target binding and the critical role of planarity in enhancing biological activity.

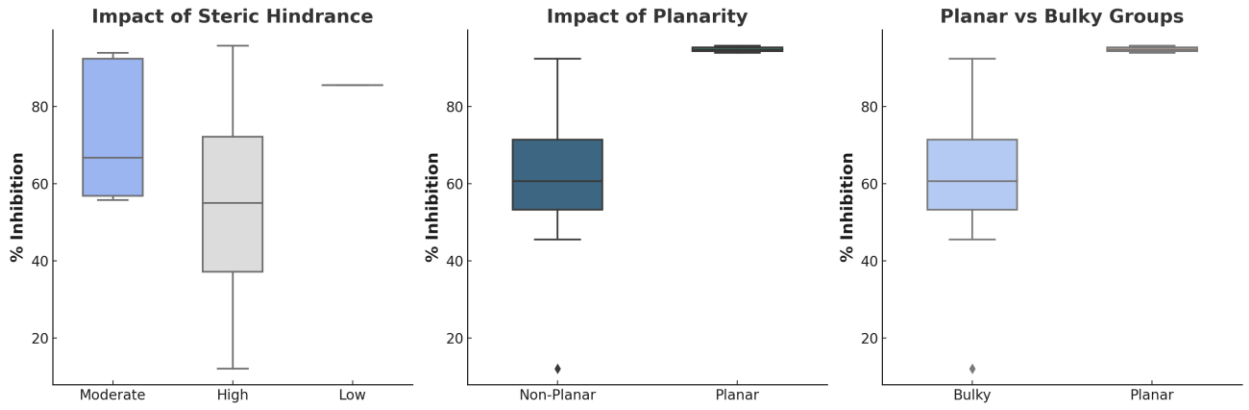

Figure S11: Impact of molecular features on % inhibition: (a) Moderate steric hindrance favors higher activity, while high steric hindrance disrupts binding efficiency; (b) planar compounds achieve consistently high activity, highlighting the importance of molecular planarity; (c) planar compounds outperform bulky groups, demonstrating the critical role of planarity in enhancing biological activity.

Planar structures with minimal steric hindrance, such as those in **4i** and **4j**, are optimal for achieving high % inhibition due to their ability to facilitate π-π stacking interactions. Compounds with moderate steric bulk (e.g., Br, F) retain high activity, balancing steric and electronic effects. However, bulky substituents, such as NO_2 and OCH_3, hinder binding and reduce activity, highlighting the critical role of steric effects in optimizing biological performance.

7.7. Binding Energies and Molecular Interactions

The relationship between binding free energies (BFE) and % inhibition was analyzed to assess the strength of molecular interactions between the compounds and the target enzyme. Binding free energy values (BFE, in kcal/mol) serve as an indicator of the binding strength, where more negative values reflect stronger interactions. These are further supported by binding affinity (AFF) values in pK units, which describe the thermodynamic favorability of binding.

Table S11 summarizes the BFE and affinity values for all compounds. Compounds with the most favorable binding energies include **4j** (-7.38 ± 0.82 kcal/mol), **4e** (-7.23 ± 0.64 kcal/mol), **4g** (-7.09 ± 0.63 kcal/mol), **4i** (-7.10 ± 0.88 kcal/mol), and the standard control **Acarbose** (-7.41 ± 0.79

kcal/mol). These compounds exhibit high % inhibition, exceeding 84%, highlighting the correlation between stronger binding (lower BFE) and increased biological activity.

7.8 HOMO-LUMO Gap Analysis

The HOMO-LUMO energy gaps (ΔE) of the synthesized compounds were calculated using the ωB97X-D/def2-tzvpp level of theory to understand their electronic properties and potential reactivity. The ΔE values ranged from **7.24 eV** to **8.09 eV**, reflecting variations in electronic excitation thresholds across the series. In theory, lower ΔE values correspond to higher electronic reactivity, which could enhance the compounds' interactions with the α-glucosidase enzyme. However, the data reveals that ΔE alone is not sufficient to predict inhibitory activity.

A lack of strong correlation between ΔE and biological activity was observed. For instance, compound **4c**, with the lowest ΔE value (7.24 eV), exhibited only moderate inhibition (45.51 ± 7.45%). Similarly, compound **4h**, with a ΔE of 7.50 eV, demonstrated minimal activity (14.33 ± 7.47%). In contrast, highly active compounds such as **4e** (92.35 ± 2.52%) and **4i** (88.64 ± 0.78%) displayed higher ΔE values of 8.03 eV and 7.62 eV, respectively. These findings suggest that while electronic properties like ΔE are important, other factors, including steric effects, molecular planarity, and binding dynamics, play a significant role in determining biological activity.

The analysis also highlights the role of molecular planarity in enhancing inhibitory potential. Planar compounds, such as **4i** (naphthalene) and **4j** (benzylidene), achieved high % inhibition values (88.64% and 93.84%, respectively) with moderate ΔE values (7.62 and 8.01 eV). These results suggest that planarity facilitates stronger π-π stacking interactions with the enzyme target, contributing to their biological efficacy. Similarly, halogen-substituted compounds like **4e** (3-Br-

Ph) and **4g** (2-F-Ph) also demonstrated favorable ΔE values (8.03 and 8.04 eV, respectively) and high inhibitory activity, highlighting the balanced effects of electronic and steric factors.

The control compound **Acarbose**, with an IC_{50} of 45.78 ± 1.95 μM, serves as a benchmark in this study. Its ΔE value is not applicable, reinforcing the notion that inhibitory activity depends on a complex interplay of electronic, steric, and structural properties.

7.10 MEP Correlation Analysis

Molecular Electrostatic Potential (MEP) maps were generated for all synthesized compounds to visualize charge distribution and identify regions of electrophilicity and nucleophilicity, which are critical for interactions with the α-glucosidase enzyme. The correlation between these MEP features and biological activity (% inhibition) was analyzed to uncover trends in the structure-activity relationship (SAR).

The MEP maps revealed that compounds with balanced charge distributions, where nucleophilic and electrophilic regions were optimally positioned, exhibited higher inhibitory activity. In contrast, uneven or poorly localized charge distributions negatively impacted binding interactions, resulting in lower activity. Key insights for each compound are summarized in Table S12 below.

Balanced Charge Distribution: Compounds like **4e**, **4g**, and **4i** demonstrated optimal MEP features, correlating with their high % inhibition values. These compounds exhibited well-positioned electrophilic and nucleophilic regions that enhance binding interactions with the enzyme active site.

Localized vs. Uneven Charges: Compounds with uneven or poorly localized charge distributions, such as **4h** (14.33 ± 7.47%), exhibited significantly lower activity. This highlights the negative impact of disrupted binding potential on enzyme inhibition.

Nucleophilic Enhancements: The nucleophilic and electrophilic regions in **4i** and **4j** provided balanced charge distributions, contributing to their excellent inhibitory activity (88.64% and 93.84%, respectively).

Halogen Substituents: The presence of Br and F in **4e** and **4g** enhances electrophilicity, enabling complementary interactions with the enzyme's active site. This supports their high inhibition values (92.35% and 85.69%, respectively).

Control Compound: Acarbose served as a reference and demonstrated the importance of optimized charge distributions, highlighting the interplay between MEP features and inhibitory activity.

Table S12. Summary of MEP features and their correlation with α-glucosidase inhibitory activity (% inhibition). Compounds with balanced charge distributions exhibit higher activity, while uneven charge distributions negatively impact binding interactions and biological activity.

Compound	Key MEP Features	% Inhibition	Observations
4a	Balanced nucleophilic and electrophilic regions	66.71 ± 4.27%	Moderate activity, charge distribution supports binding.
4b	Nucleophilic regions localized to pyridine ring	51.65 ± 4.72%	Lower activity likely due to reduced interaction area.
4c	Localized nucleophilic regions near nitro group	45.51 ± 7.45%	Limited binding potential due to uneven charge.
4d	Distributed nucleophilic region near nitro group	59.86 ± 2.60%	Moderate activity, better charge balance than 4c.
4e	Enhanced electrophilic region due to Br substituent	92.35 ± 2.52%	High activity, optimal MEP distribution.
4f	Balanced charge distribution near hydroxyl group	55.75 ± 1.91%	Moderate activity with potential steric hindrance.
4g	Localized nucleophilic region near fluorine atom	85.69 ± 1.59%	High activity, complementary MEP features.
4h	Uneven charge distribution across the molecule	14.33 ± 7.47%	Poor activity due to disrupted binding potential.
4i	Balanced nucleophilic and electrophilic regions	88.64 ± 0.78%	High activity, complementary MEP features.
4j	Balanced charge distribution near phenyl group	93.84 ± 1.49%	High activity, effective MEP and steric features.

The MEP analysis emphasizes that balanced charge distributions, particularly accessible electrophilic and nucleophilic regions, are critical for effective enzyme inhibition. While other factors, such as steric effects and binding dynamics, play a role, these findings underscore the importance of integrating MEP features into structure-activity relationship (SAR) models for designing potent inhibitors.

8. NMR Spectra

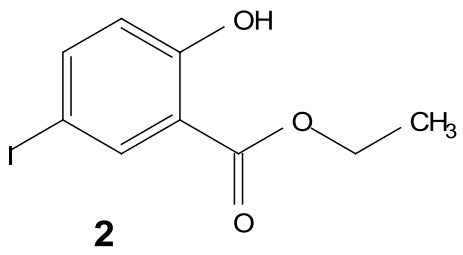
OH
I
O
CH3
O

2

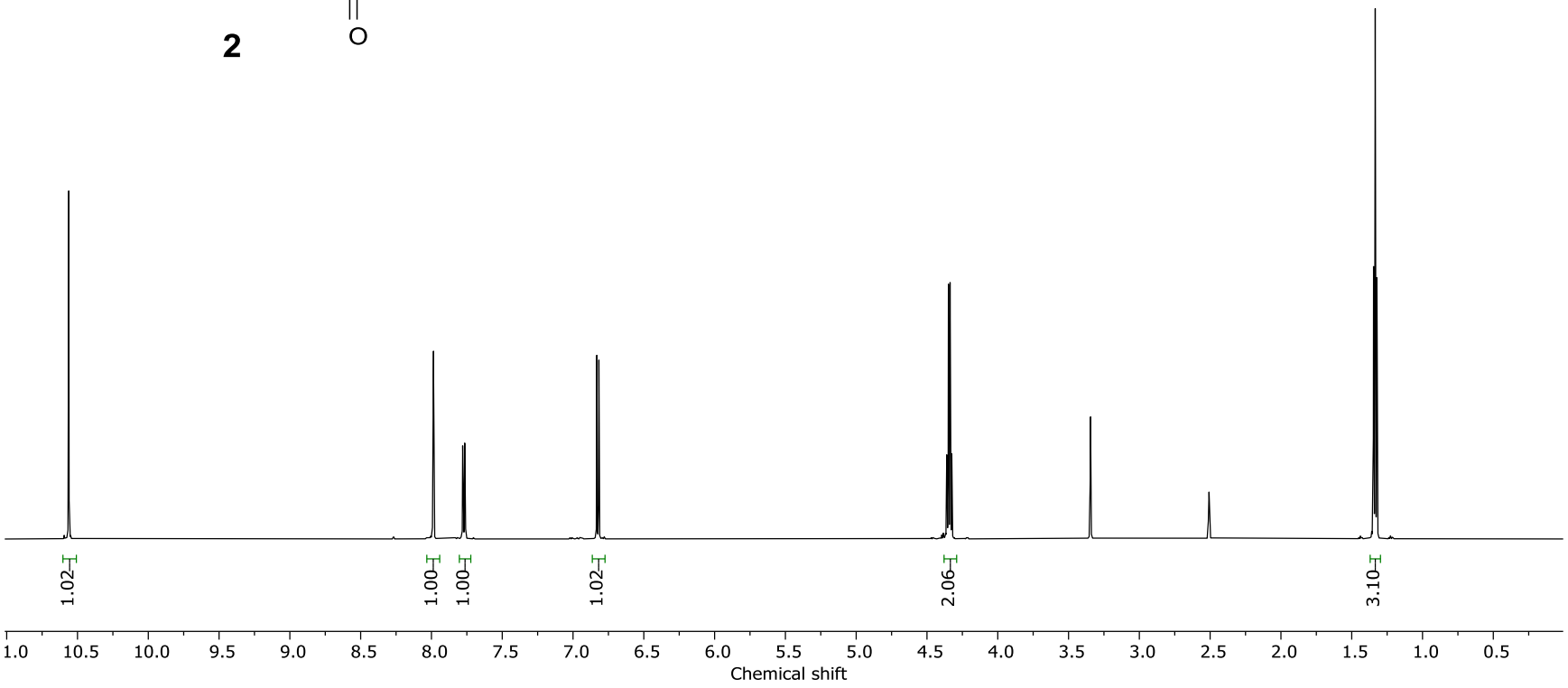
1.02
1.00
1.00
1.02
2.06
3.10
1.0 10.5 10.0 9.5 9.0 8.5 8.0 7.5 7.0 6.5 6.0 5.5 5.0 4.5 4.0 3.5 3.0 2.5 2.0 1.5 1.0 0.5
Chemical shift

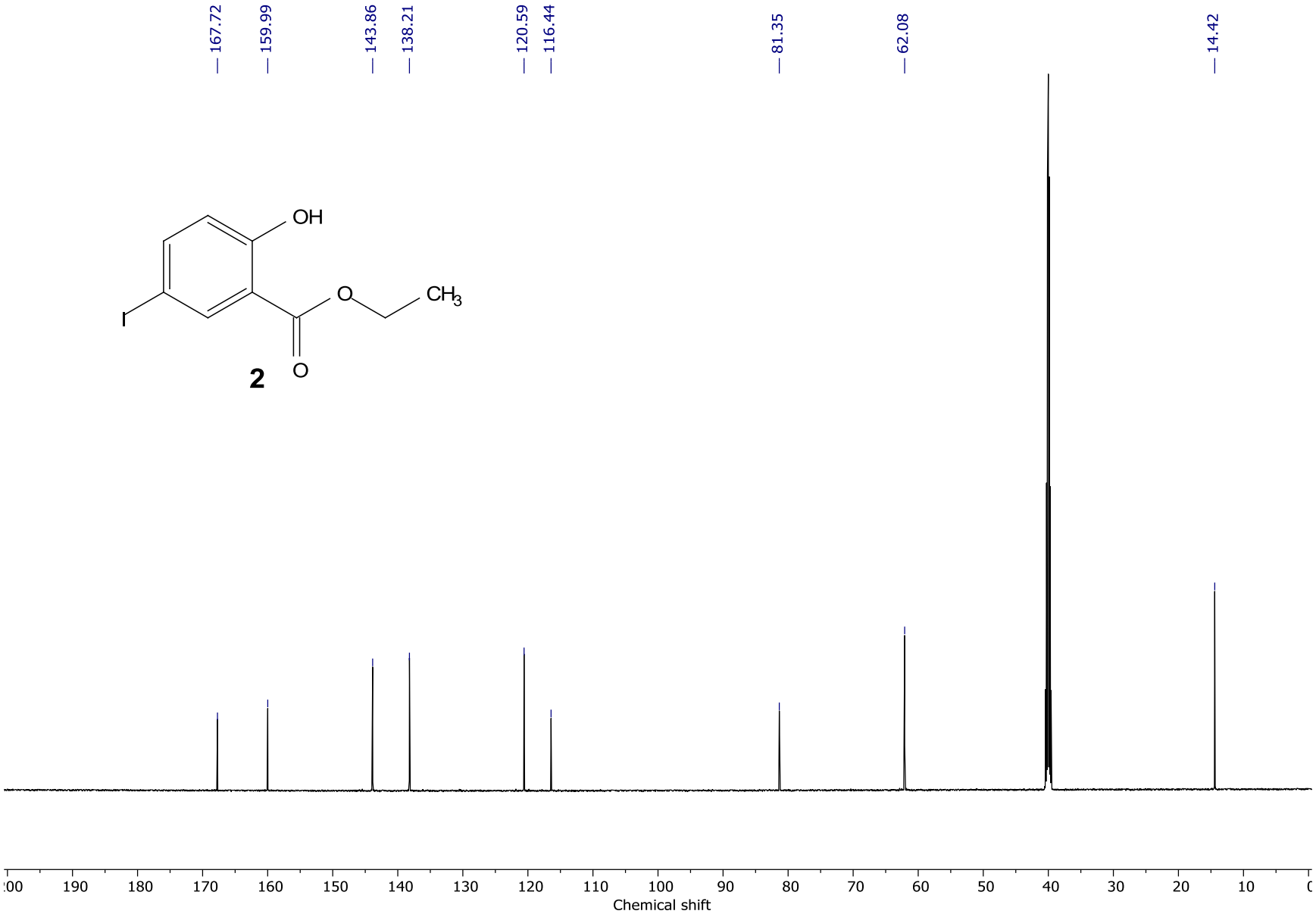
167.72
159.99
143.86
138.21
120.59
116.44
81.35
62.08
14.42
OH
O
CH3
I
O
2
190
180
170
160
150
140
130
120
110
100
90
80
70
60
50
40
30
20
10
Chemical shift

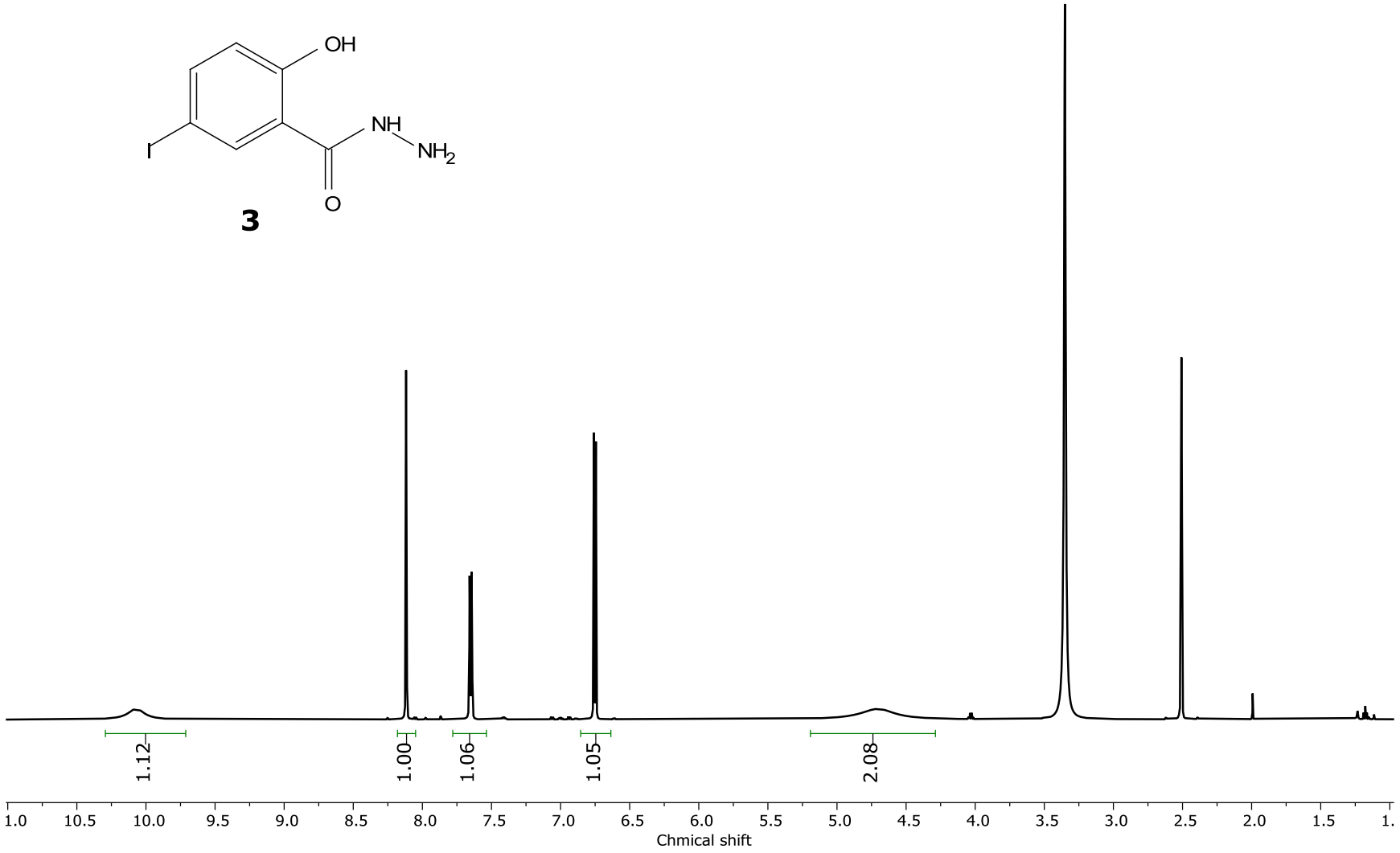
OH
NH
NH2
I
O
3
1.12
1.00
1.06
1.05
2.08
1.0
10.5
10.0
9.5
9.0
8.5
8.0
7.5
7.0
6.5
6.0
5.5
5.0
4.5
4.0
3.5
3.0
2.5
2.0
1.5
Chmical shift

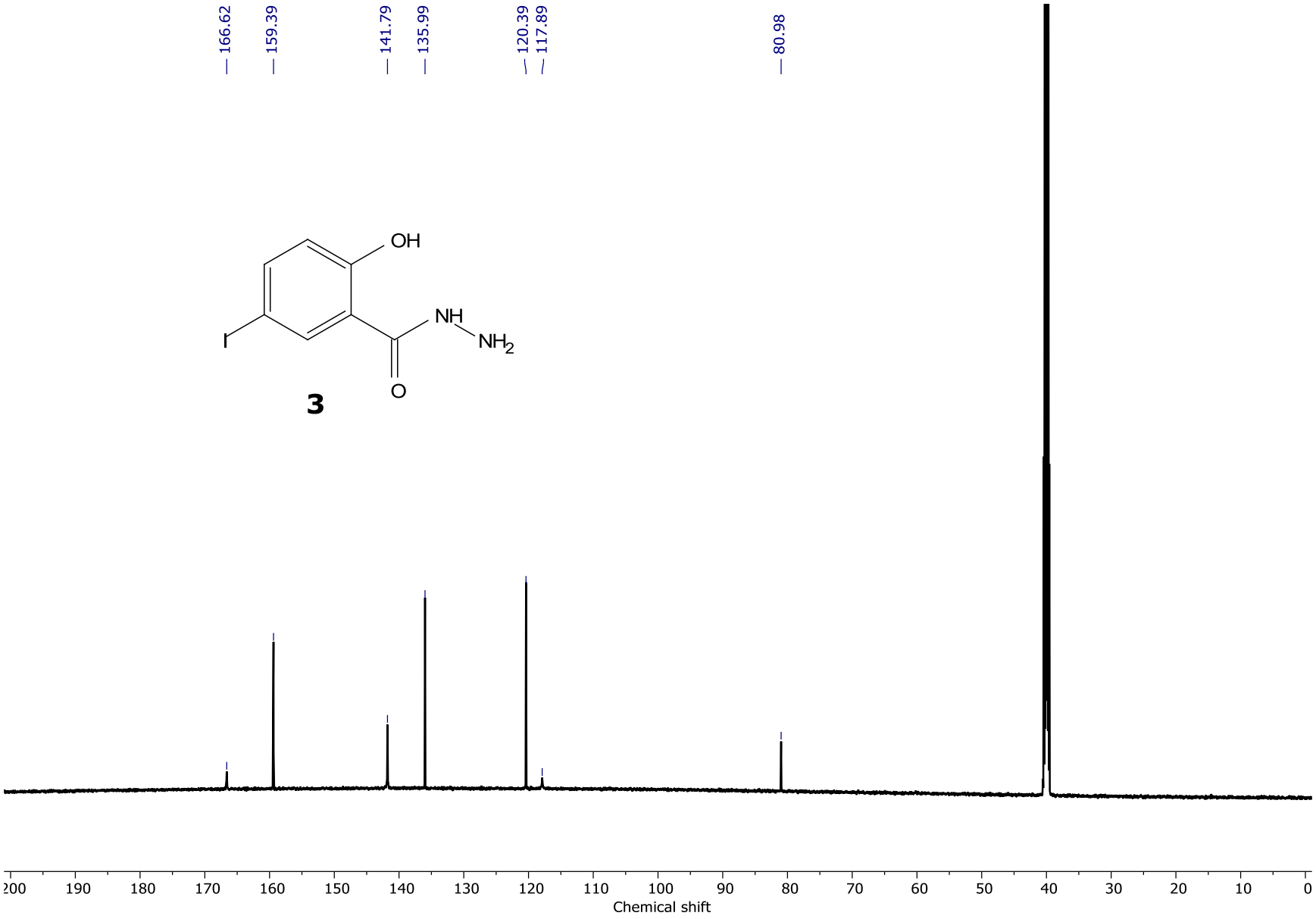
166.62
159.39
141.79
135.99
120.39
117.89
80.98
OH
NH
NH2
I
O
3
200
190
180
170
160
150
140
130
120
110
100
90
80
70
60
50
40
30
20
10
0
Chemical shift

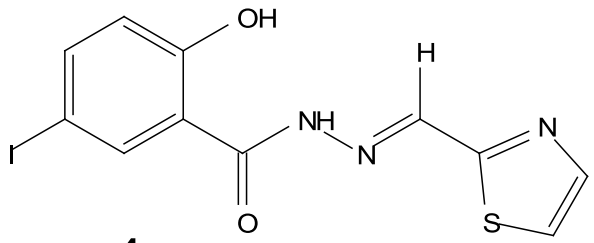
OH
H
NH
N
N
I
O
S

4a

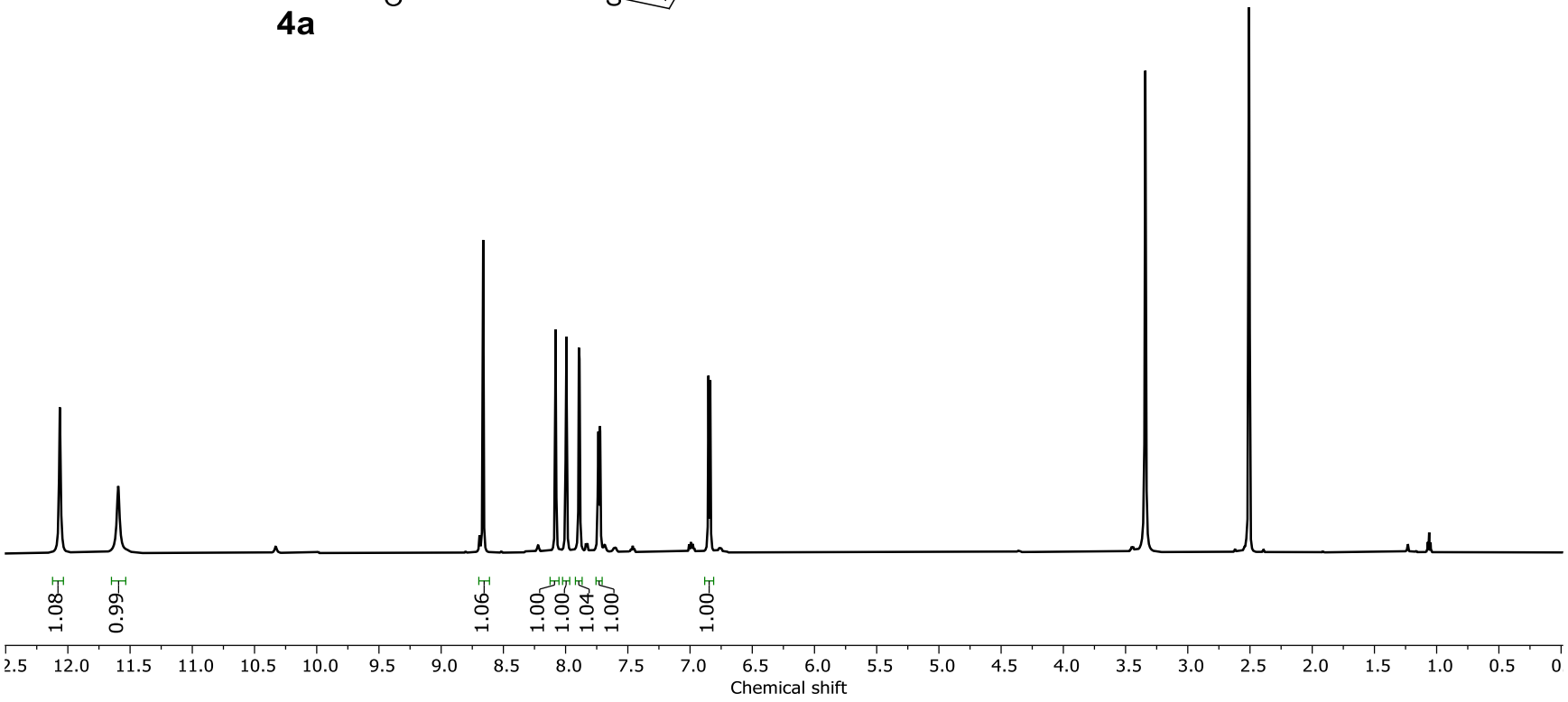
1.08
0.99
1.06
1.00
1.00
1.04
1.00
1.00
2.5 12.0 11.5 11.0 10.5 10.0 9.5 9.0 8.5 8.0 7.5 7.0 6.5 6.0 5.5 5.0 4.5 4.0 3.5 3.0 2.5 2.0 1.5 1.0 0.5 0
Chemical shift

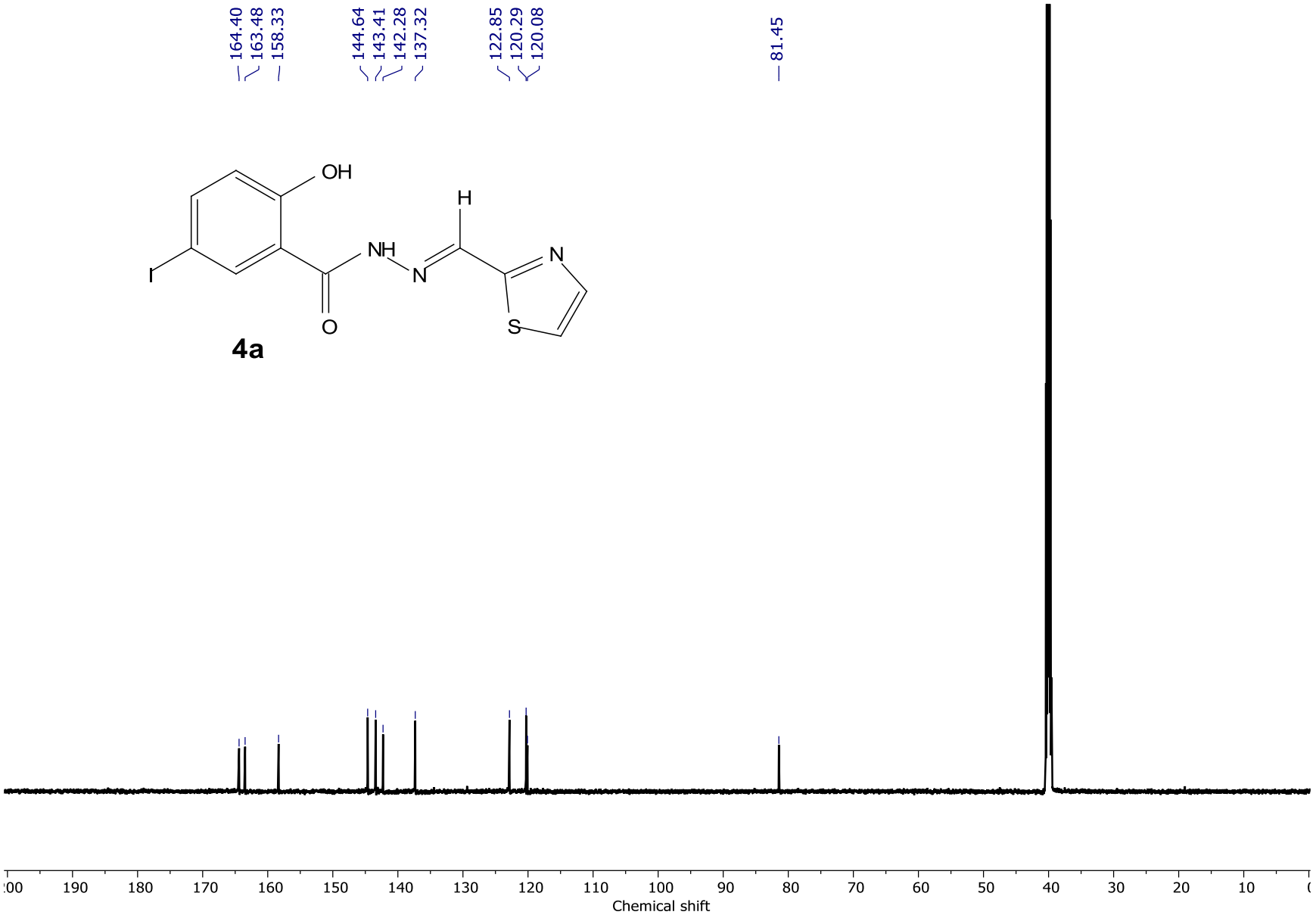
164.40
163.48
158.33
144.64
143.41
142.28
137.32
122.85
120.29
120.08
81.45
OH
H
NH
N
N
I
O
S
4a
Chemical shift

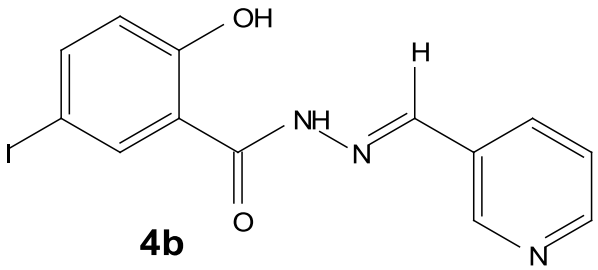
OH
H
NH
N
I
O
N

4b

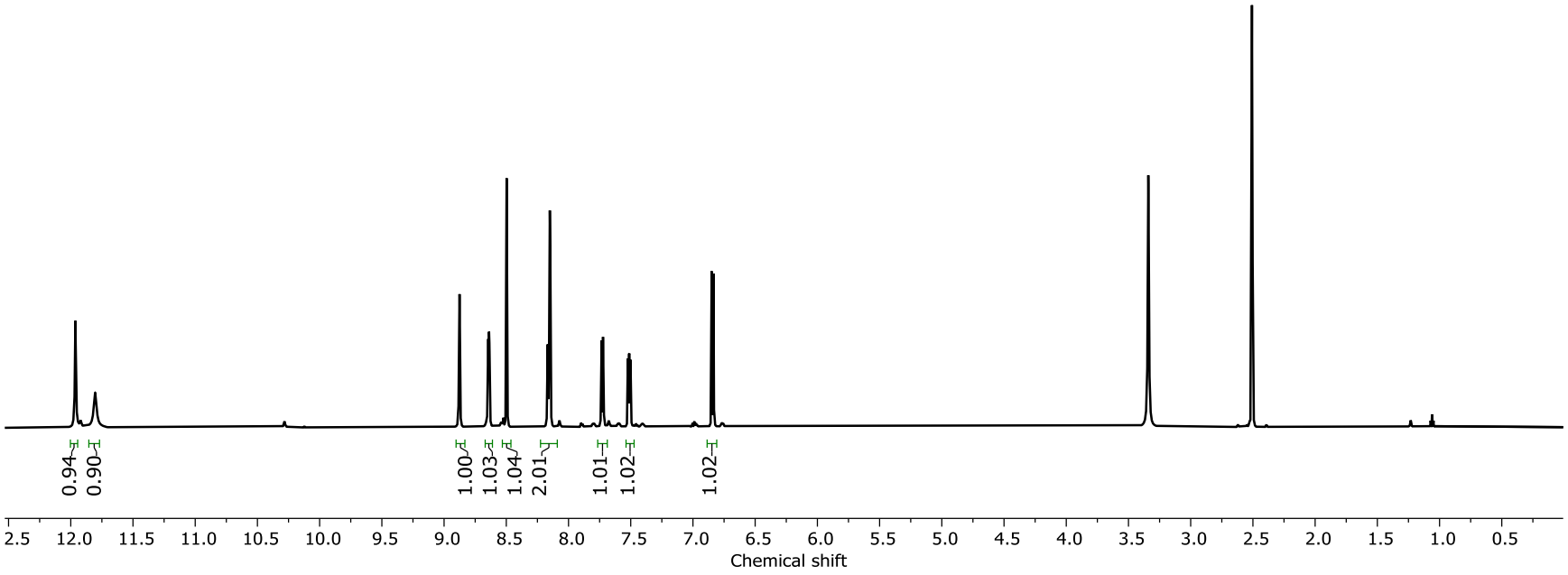
0.94
0.90
1.00
1.03
1.04
2.01
1.01
1.02
1.02
2.5 12.0 11.5 11.0 10.5 10.0 9.5 9.0 8.5 8.0 7.5 7.0 6.5 6.0 5.5 5.0 4.5 4.0 3.5 3.0 2.5 2.0 1.5 1.0 0.5
Chemical shift

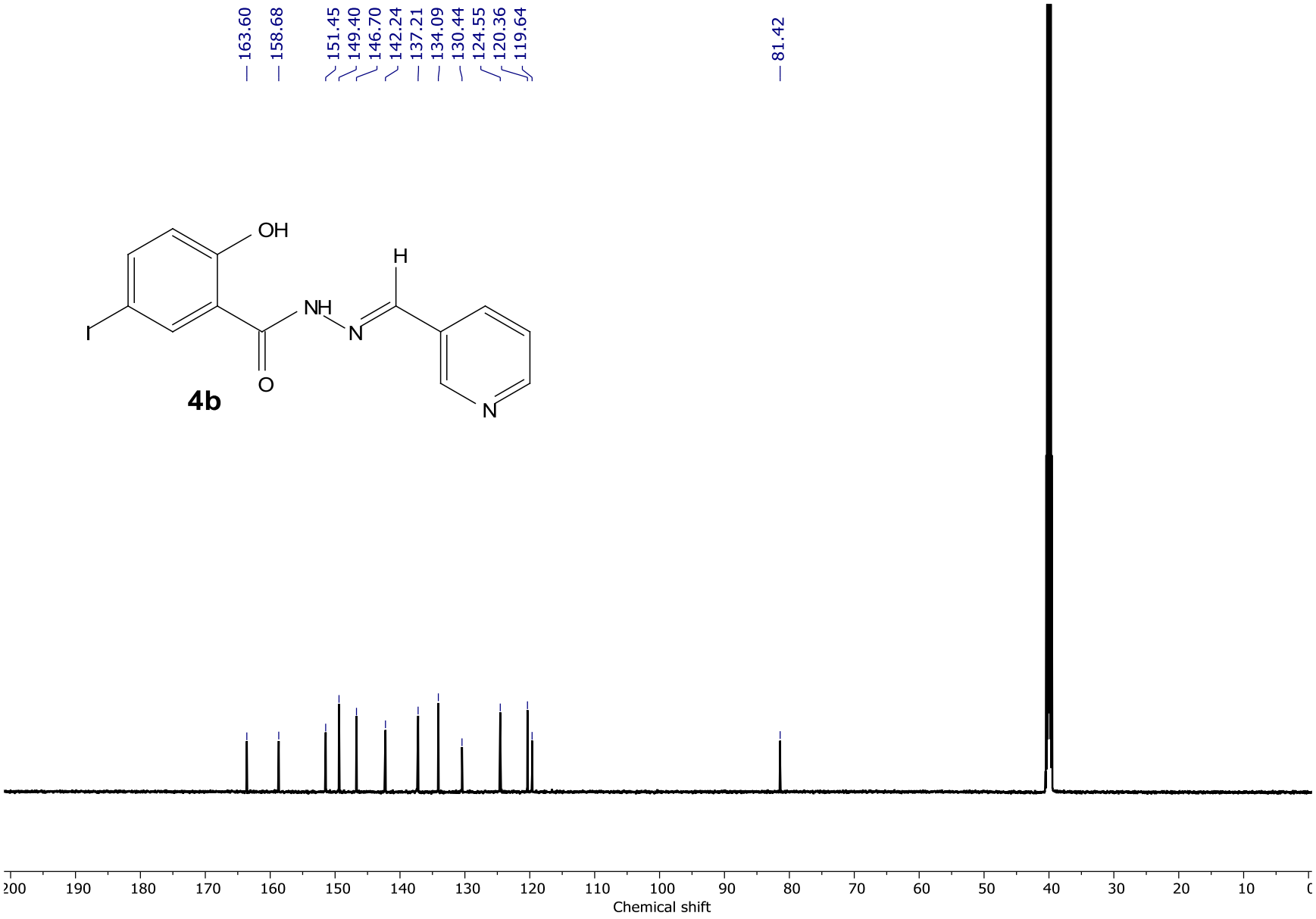
163.60
158.68
151.45
149.40
146.70
142.24
137.21
134.09
130.44
124.55
120.36
119.64
81.42
OH
NH
N
H
O
N
I
4b
200
190
180
170
160
150
140
130
120
110
100
90
80
70
60
50
40
30
20
10
Chemical shift

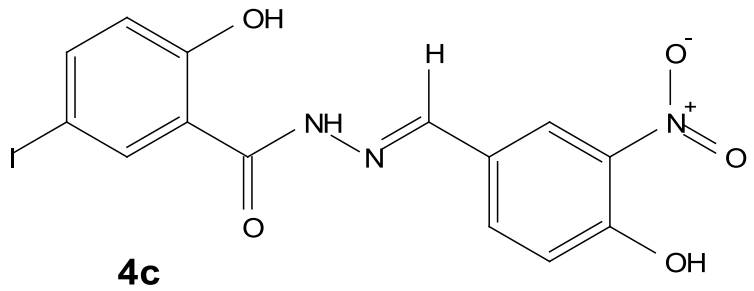
OH
H
O
-
NH
N
N
+
O
O
OH

4c

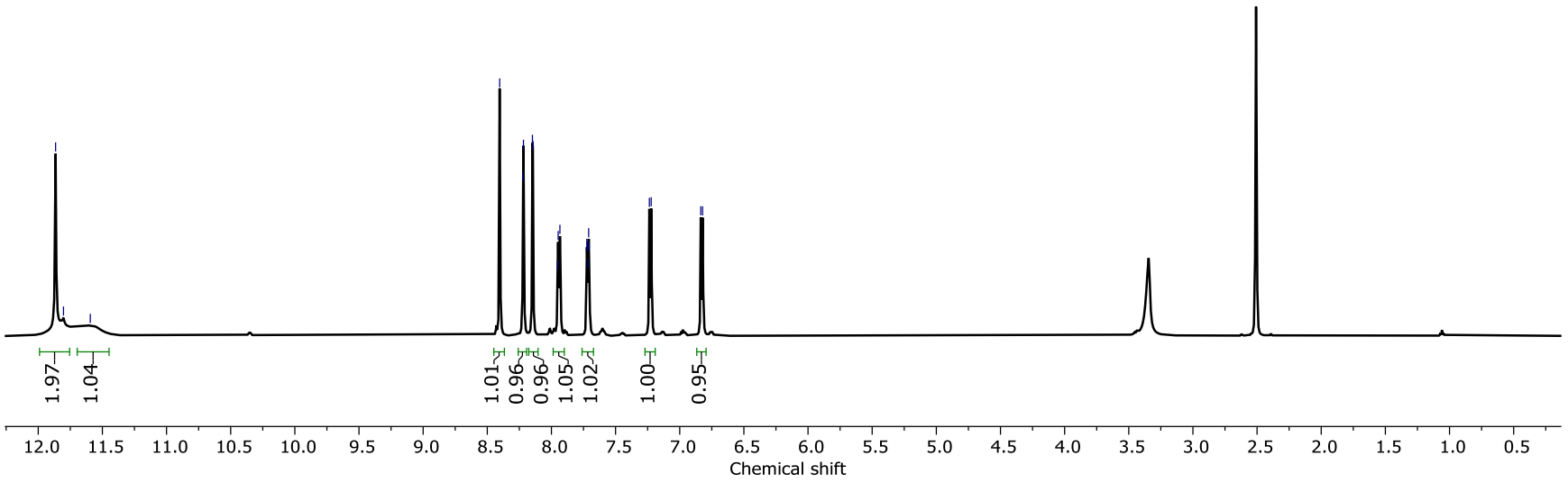
1.97
1.04
1.01
0.96
0.96
1.05
1.02
1.00
0.95
12.0
11.5
11.0
10.5
10.0
9.5
9.0
8.5
8.0
7.5
7.0
6.5
6.0
5.5
5.0
4.5
4.0
3.5
3.0
2.5
2.0
1.5
1.0
0.5
Chemical shift

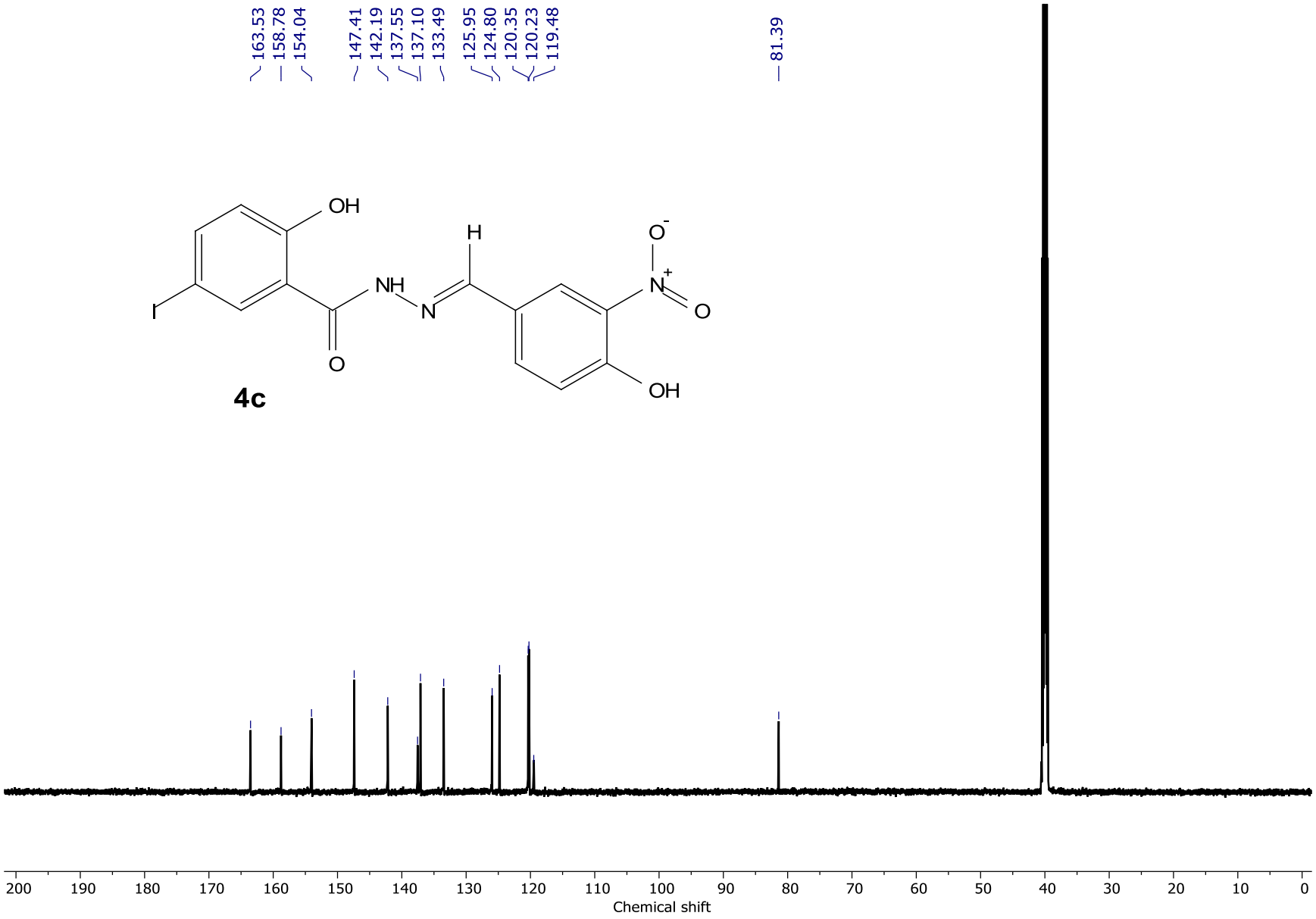
163.53
158.78
154.04
147.41
142.19
137.55
137.10
133.49
125.95
124.80
120.35
120.23
119.48
81.39
OH
H
O-
NH
N
N+
O
I
O
OH
4c
200
190
180
170
160
150
140
130
120
110
100
90
80
70
60
50
40
30
20
10
0
Chemical shift

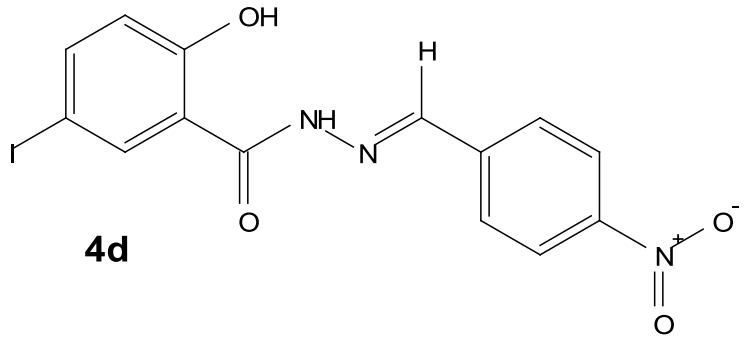
OH
H
NH
N
I
O
O
N+
O-
O

4d

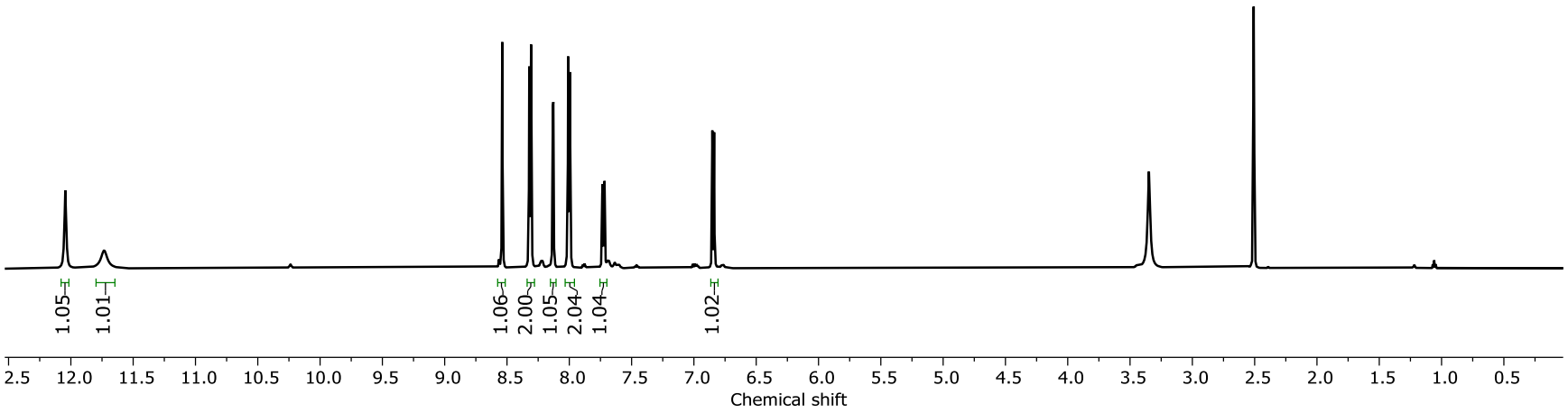
1.05
1.01
1.06
2.00
1.05
2.04
1.04
1.02
2.5 12.0 11.5 11.0 10.5 10.0 9.5 9.0 8.5 8.0 7.5 7.0 6.5 6.0 5.5 5.0 4.5 4.0 3.5 3.0 2.5 2.0 1.5 1.0 0.5
Chemical shift

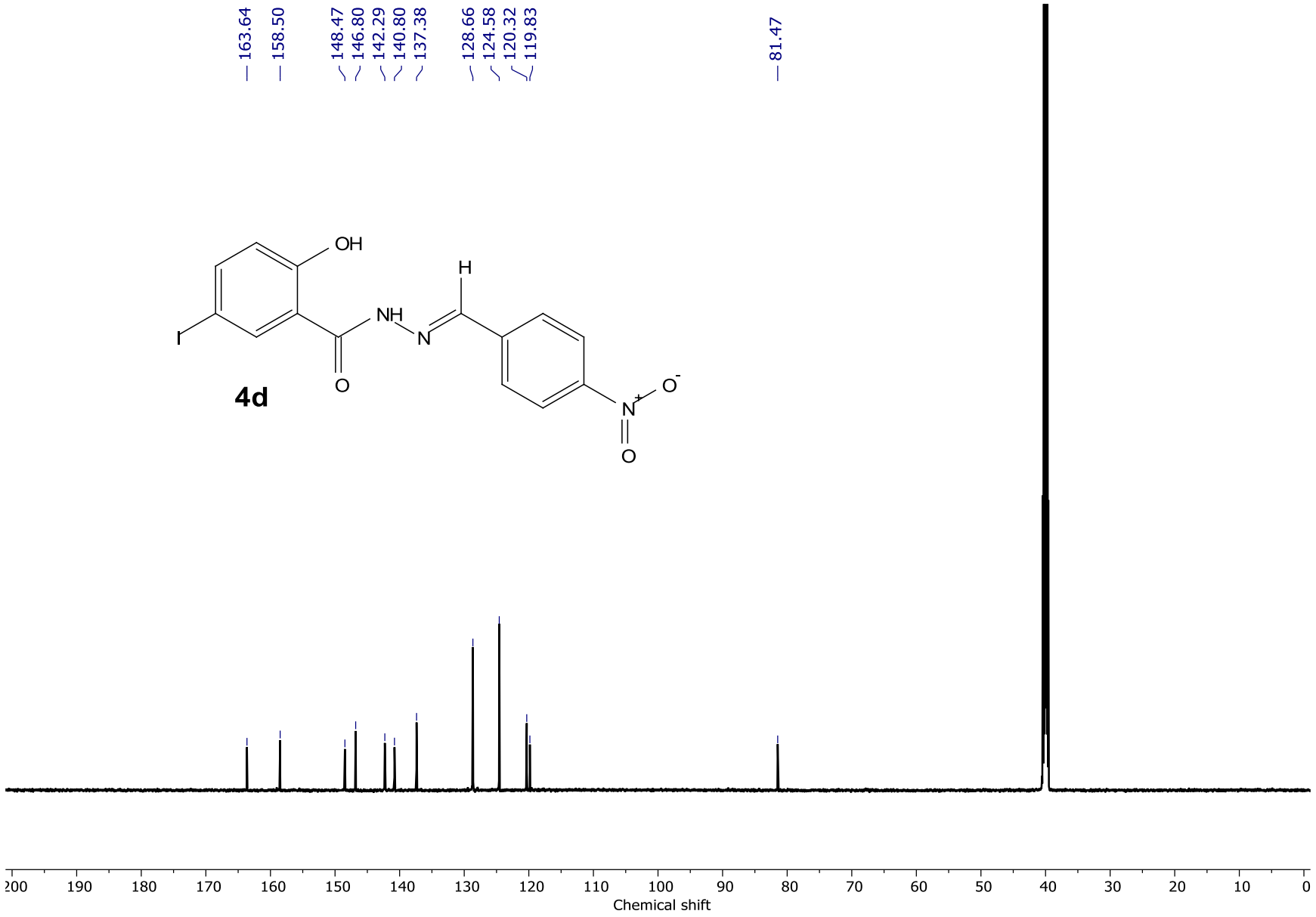
163.64
158.50
148.47
146.80
142.29
140.80
137.38
128.66
124.58
120.32
119.83
81.47
OH
H
NH
N
I
O
O
N+
O-
O
4d
200
190
180
170
160
150
140
130
120
110
100
90
80
70
60
50
40
30
20
10
0
Chemical shift

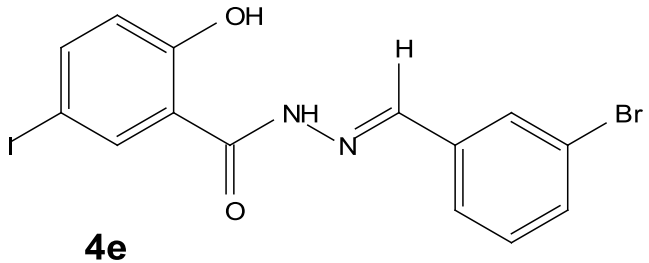
OH
H
NH
N
Br
I
O

4e

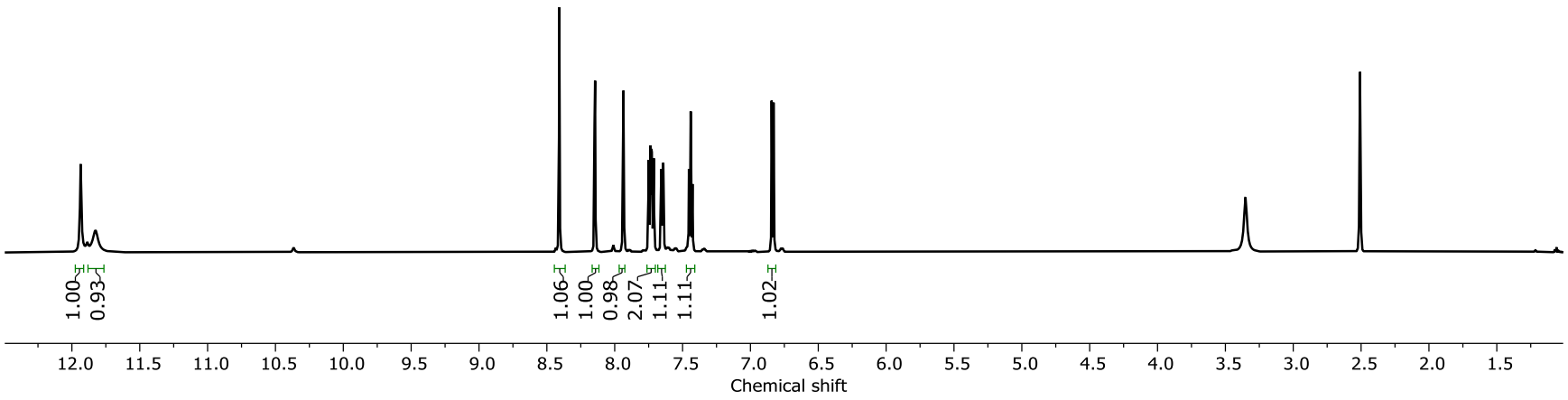
1.00
0.93
1.06
1.00
0.98
2.07
1.11
1.11
1.02
12.0
11.5
11.0
10.5
10.0
9.5
9.0
8.5
8.0
7.5
7.0
6.5
6.0
5.5
5.0
4.5
4.0
3.5
3.0
2.5
2.0
1.5
Chemical shift

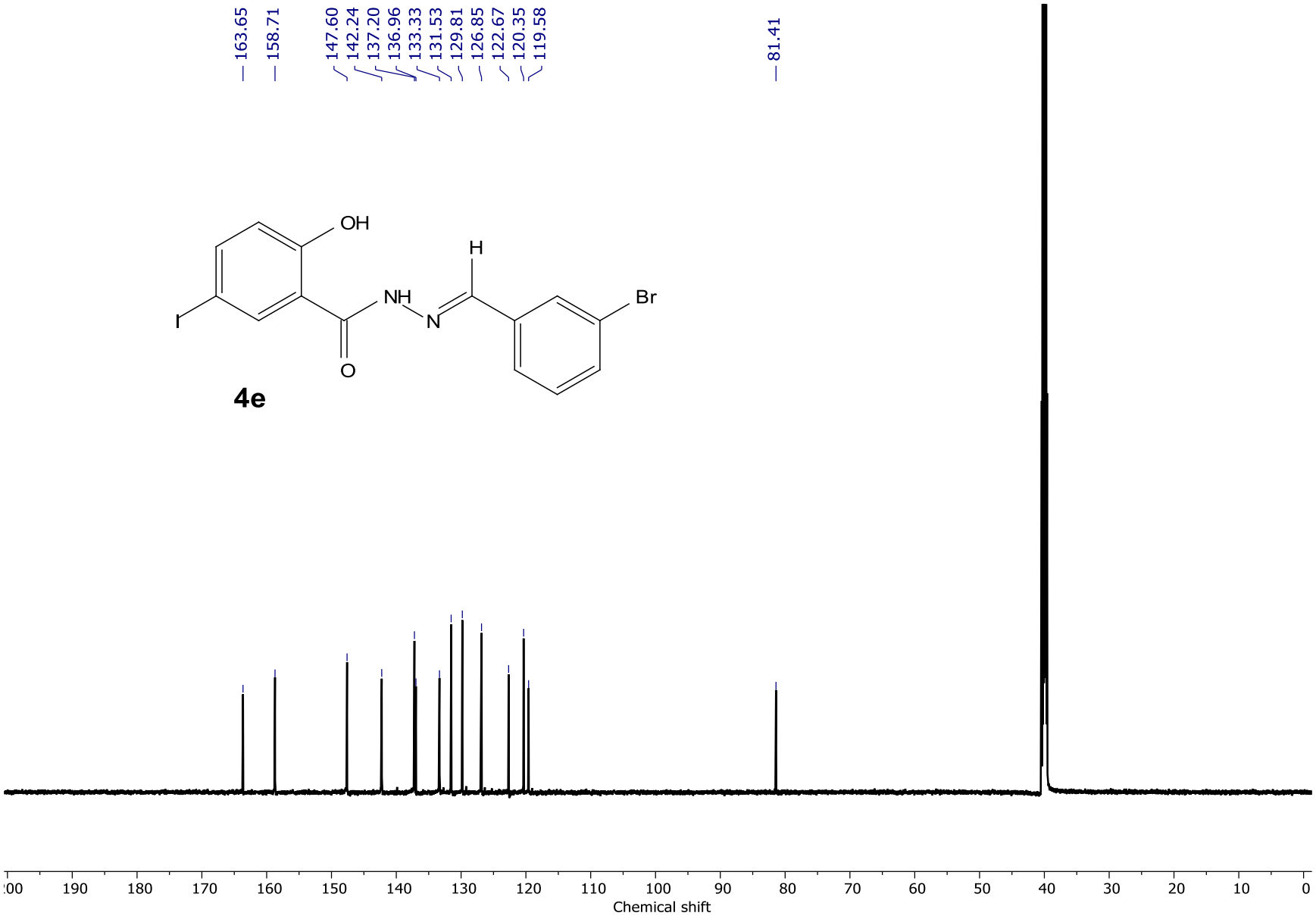
163.65
158.71
147.60
142.24
137.20
136.96
133.33
131.53
129.81
126.85
122.67
120.35
119.58
81.41
OH
H
NH
N
Br
I
O
4e
190
180
170
160
150
140
130
120
110
100
90
80
70
60
50
40
30
20
10
0
Chemical shift

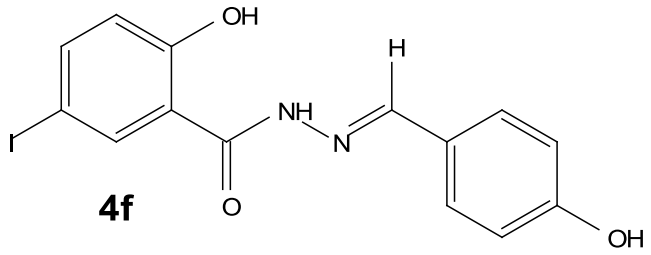
OH
H
NH
N
I
O
OH

4f

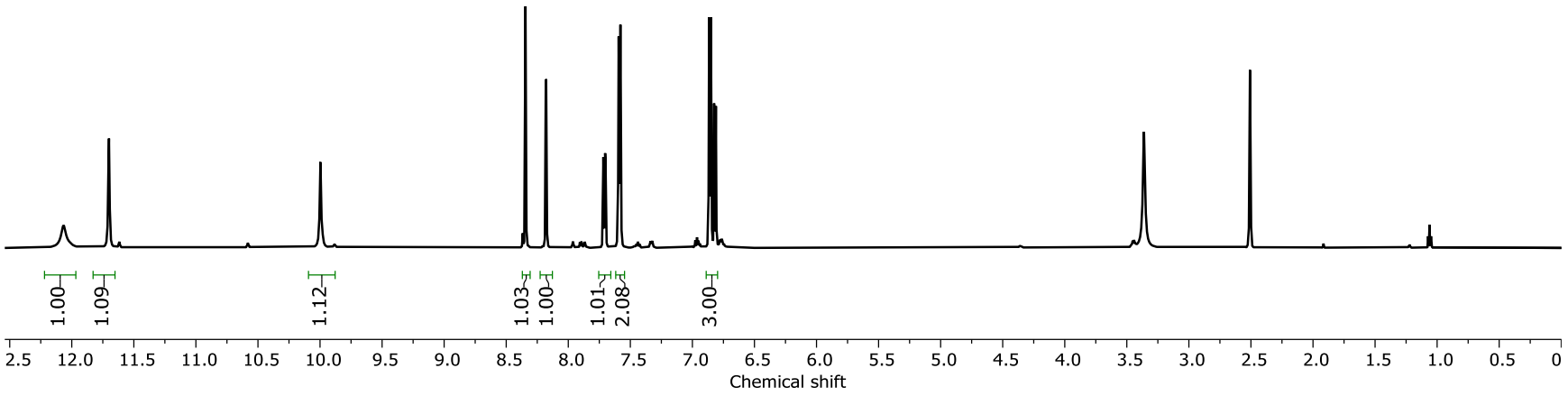
1.00
1.09
1.12
1.03
1.00
1.01
2.08
3.00
2.5 12.0 11.5 11.0 10.5 10.0 9.5 9.0 8.5 8.0 7.5 7.0 6.5 6.0 5.5 5.0 4.5 4.0 3.5 3.0 2.5 2.0 1.5 1.0 0.5 0
Chemical shift

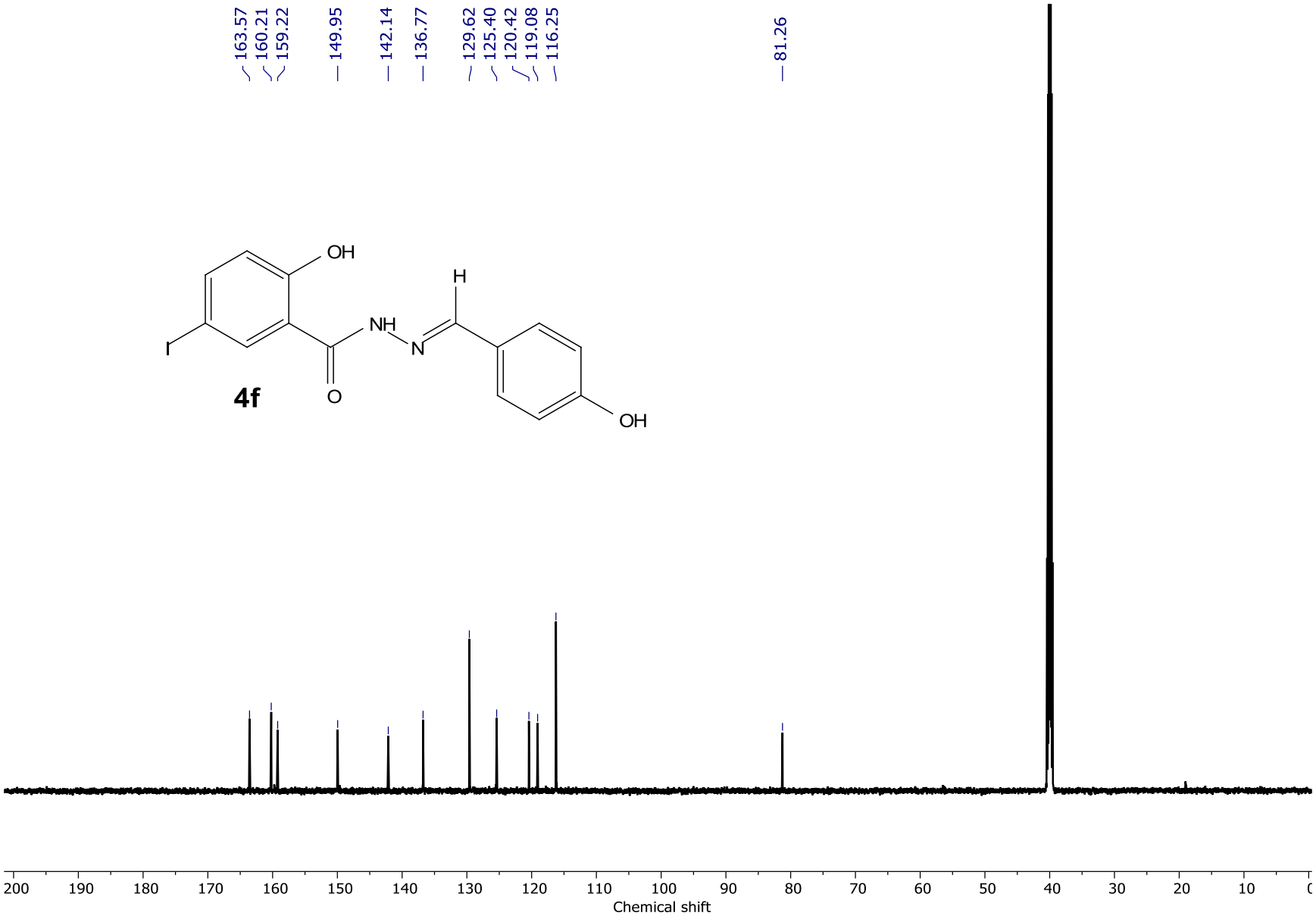
163.57
160.21
159.22
149.95
142.14
136.77
129.62
125.40
120.42
119.08
116.25
81.26
OH
H
NH
N
I
O
OH
4f
200
190
180
170
160
150
140
130
120
110
100
90
80
70
60
50
40
30
20
10
Chemical shift

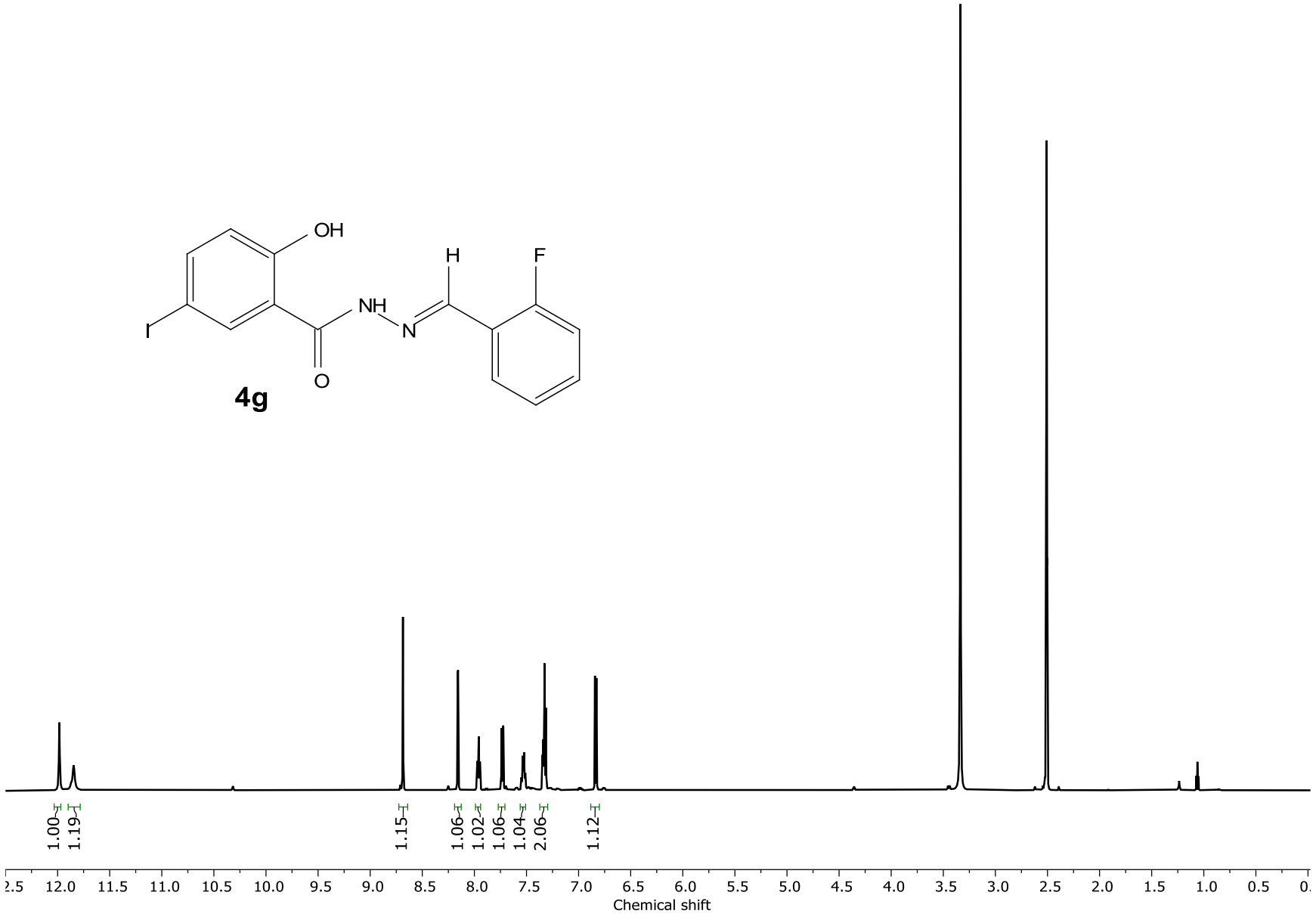
OH
H
F
NH
N
I
O
4g
1.00
1.19
1.15
1.06
1.02
1.06
1.04
2.06
1.12
Chemical shift

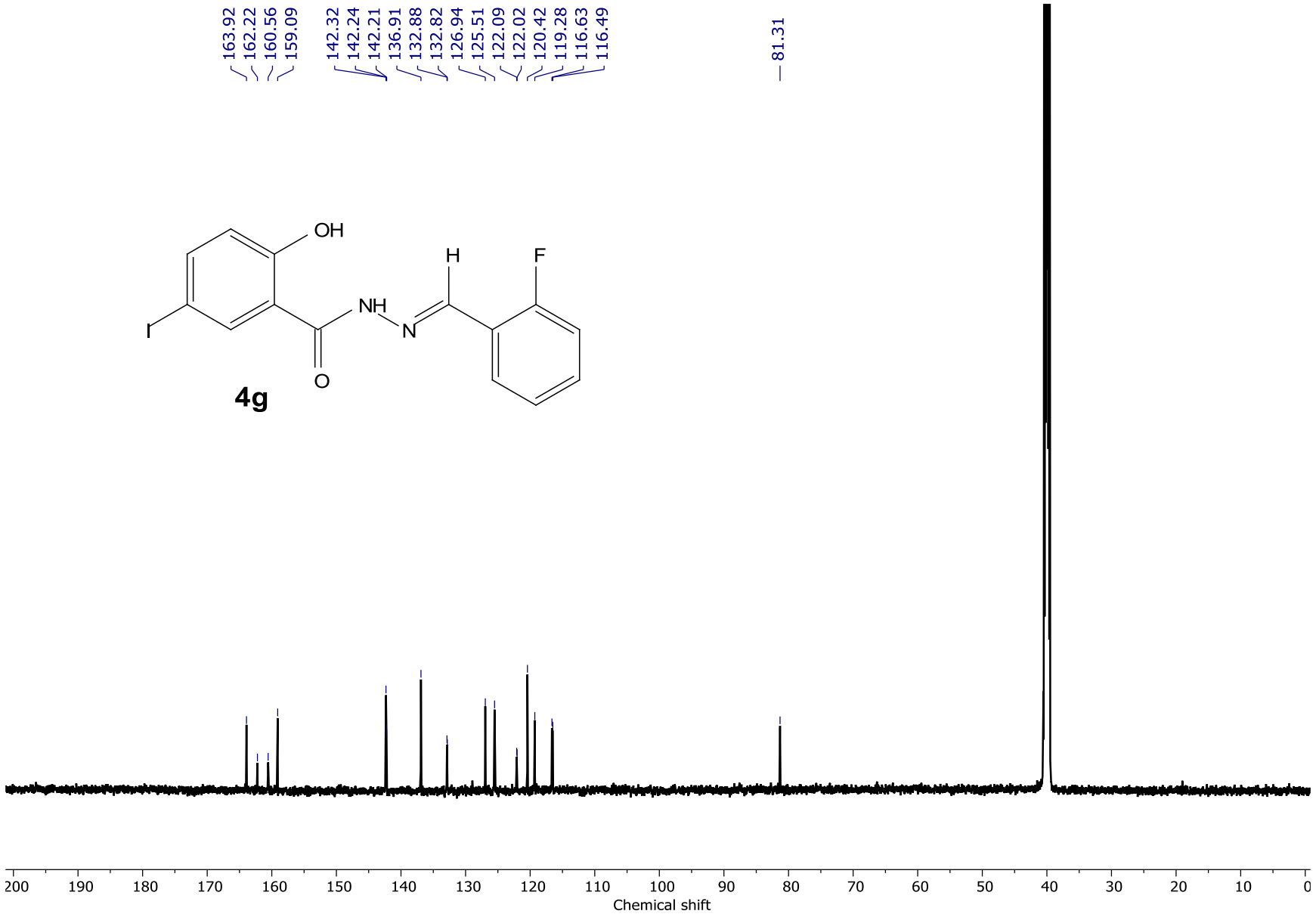
163.92
162.22
160.56
159.09
142.32
142.24
142.21
136.91
132.88
132.82
126.94
125.51
122.09
122.02
120.42
119.28
116.63
116.49
81.31
OH
H
F
NH
N
I
O
4g
200
190
180
170
160
150
140
130
120
110
100
90
80
70
60
50
40
30
20
10
0
Chemical shift

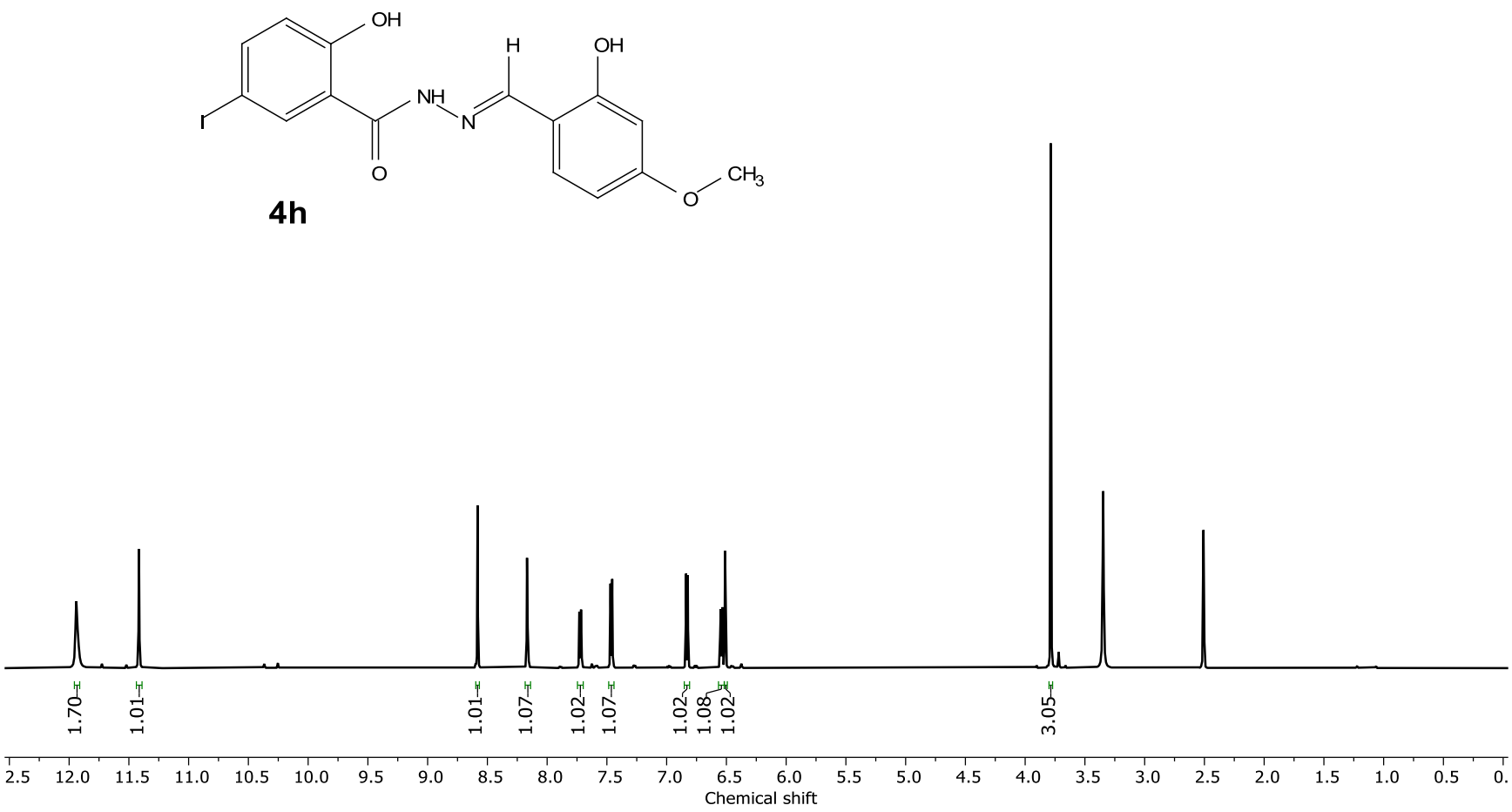
OH
H
OH
NH
N
I
O
CH3
O
4h
1.70
1.01
1.01
1.07
1.02
1.07
1.02
1.08
1.02
3.05
2.5 12.0 11.5 11.0 10.5 10.0 9.5 9.0 8.5 8.0 7.5 7.0 6.5 6.0 5.5 5.0 4.5 4.0 3.5 3.0 2.5 2.0 1.5 1.0 0.5 0.
Chemical shift

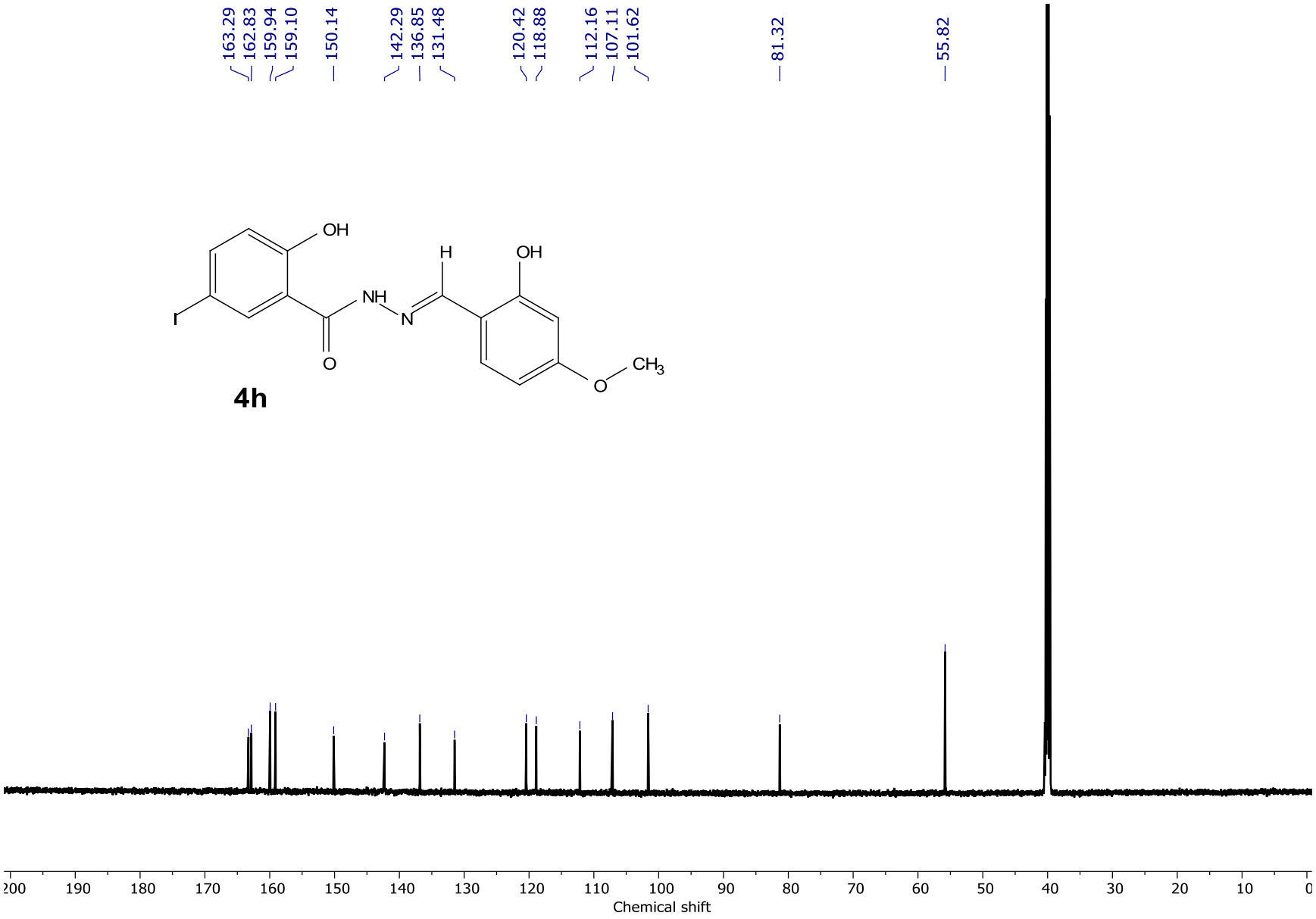
163.29
162.83
159.94
159.10
150.14
142.29
136.85
131.48
120.42
118.88
112.16
107.11
101.62
81.32
55.82
OH
H
OH
NH
N
O
CH3
O
4h
200
190
180
170
160
150
140
130
120
110
100
90
80
70
60
50
40
30
20
10
0
Chemical shift

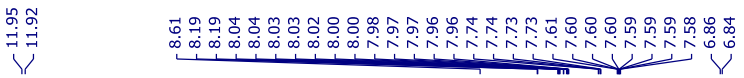
11.95
11.92
8.61
8.19
8.19
8.04
8.04
8.03
8.03
8.02
8.00
8.00
7.98
7.97
7.97
7.96
7.96
7.74
7.74
7.73
7.73
7.61
7.60
7.60
7.60
7.59
7.59
7.59
7.58
6.86
6.84

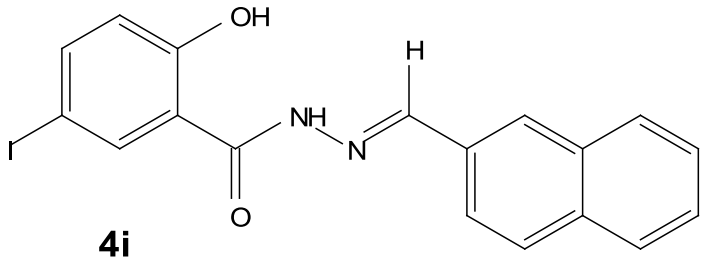
OH
H
NH
N
I
O

4i

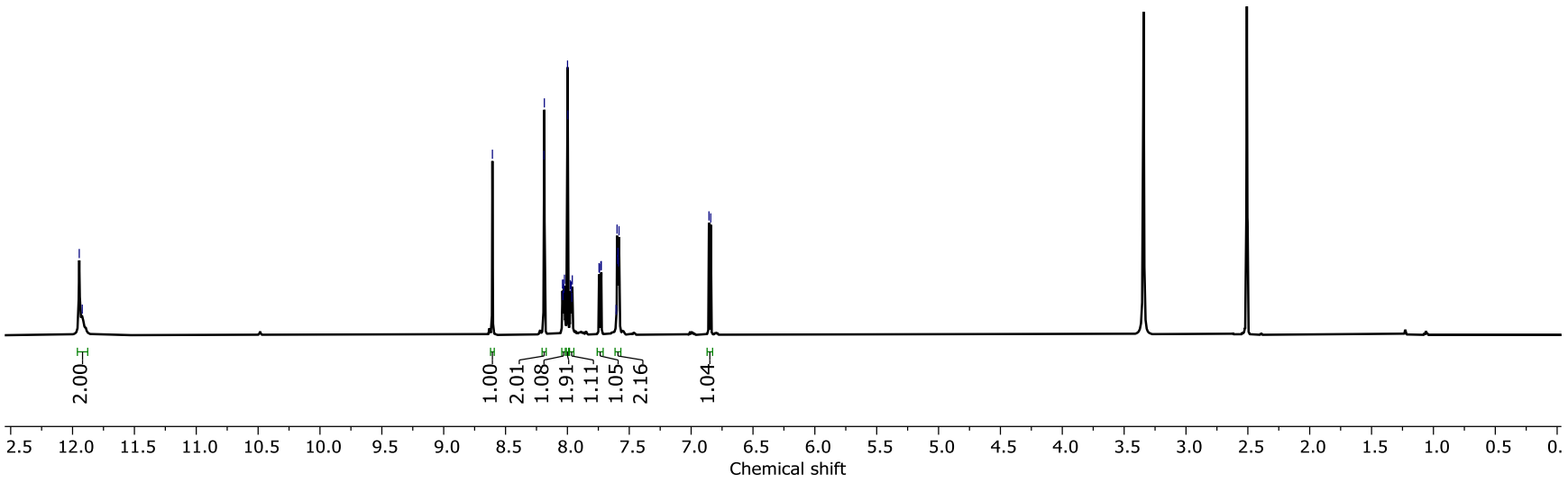
2.00
1.00
2.01
1.08
1.91
1.11
1.05
2.16
1.04
2.5
12.0
11.5
11.0
10.5
10.0
9.5
9.0
8.5
8.0
7.5
7.0
6.5
6.0
5.5
5.0
4.5
4.0
3.5
3.0
2.5
2.0
1.5
1.0
0.5
0.
Chemical shift

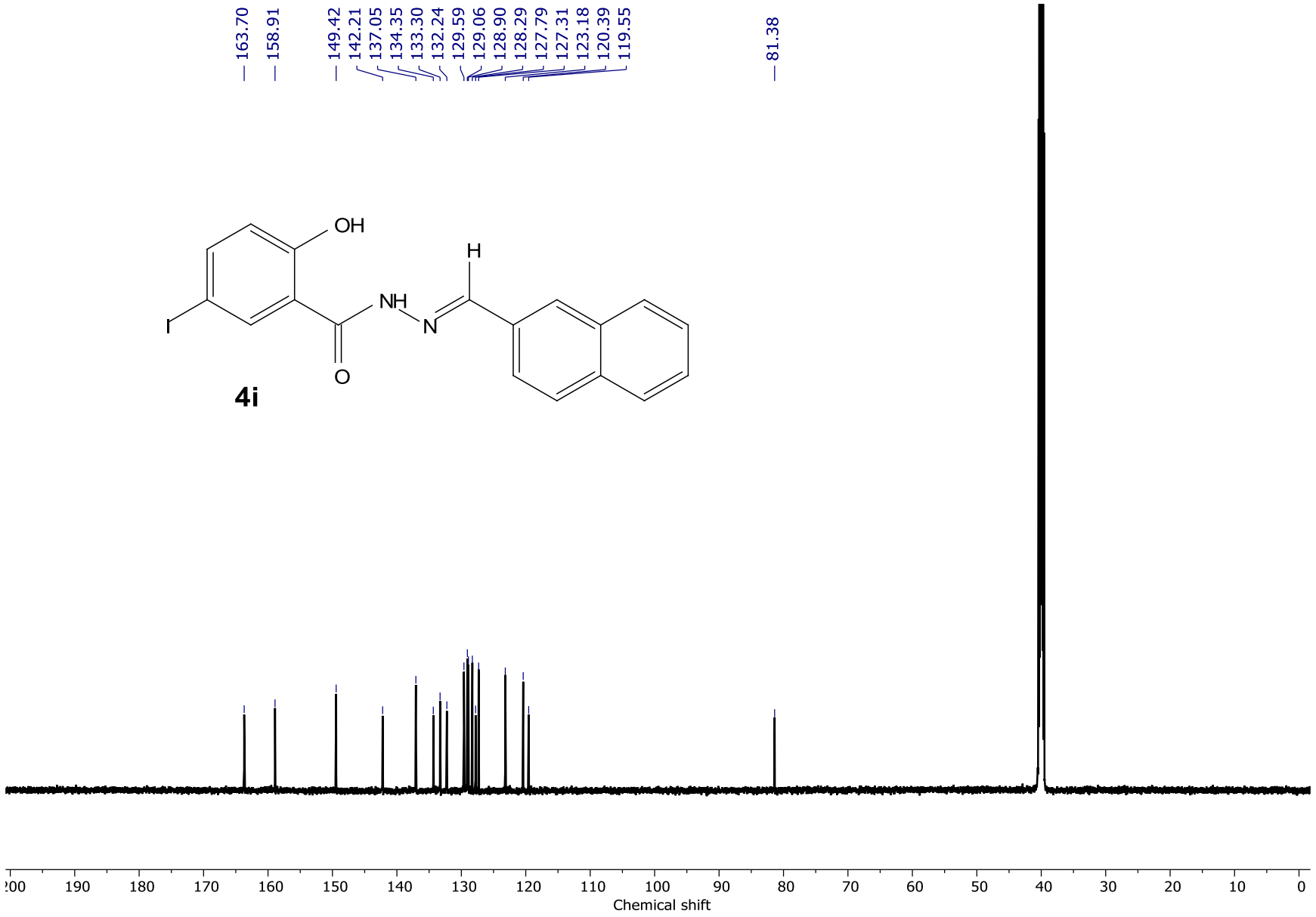
163.70
158.91
149.42
142.21
137.05
134.35
133.30
132.24
129.59
129.06
128.90
128.29
127.79
127.31
123.18
120.39
119.55
81.38
OH
H
NH
N
I
O
4i
200
190
180
170
160
150
140
130
120
110
100
90
80
70
60
50
40
30
20
10
0
Chemical shift

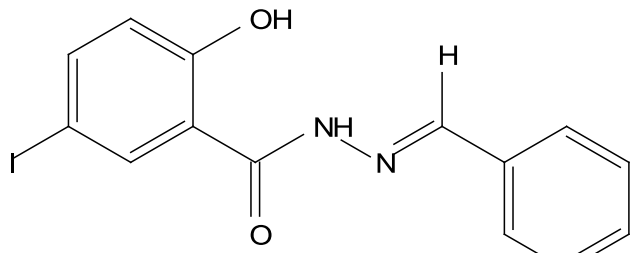
OH
H
NH
N
I
O

4i

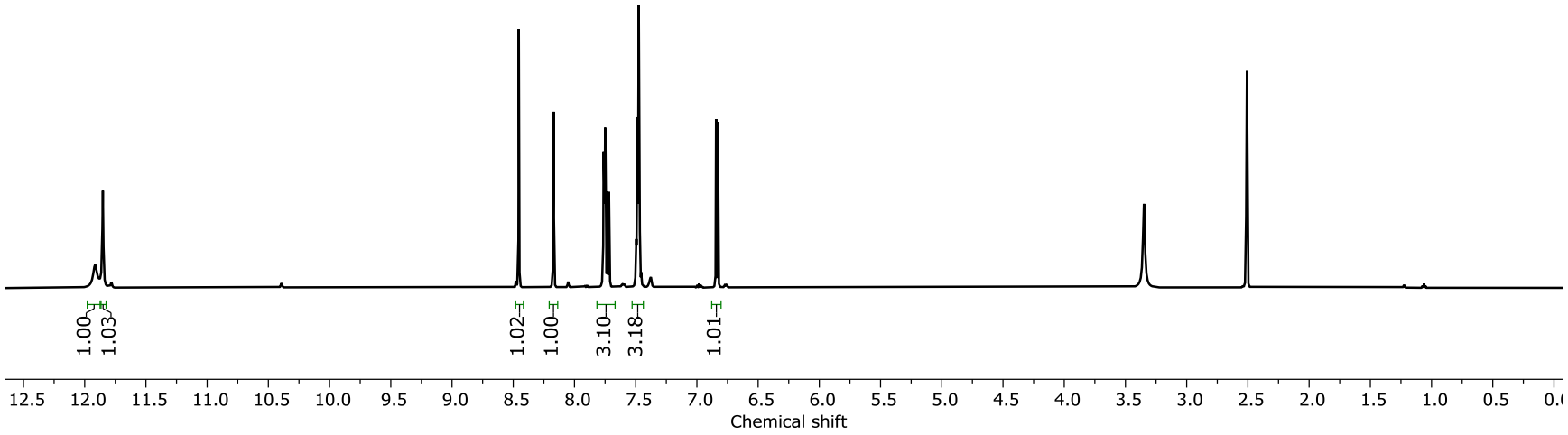
1.00
1.03
1.02
1.00
3.10
3.18
1.01
12.5 12.0 11.5 11.0 10.5 10.0 9.5 9.0 8.5 8.0 7.5 7.0 6.5 6.0 5.5 5.0 4.5 4.0 3.5 3.0 2.5 2.0 1.5 1.0 0.5
Chemical shift

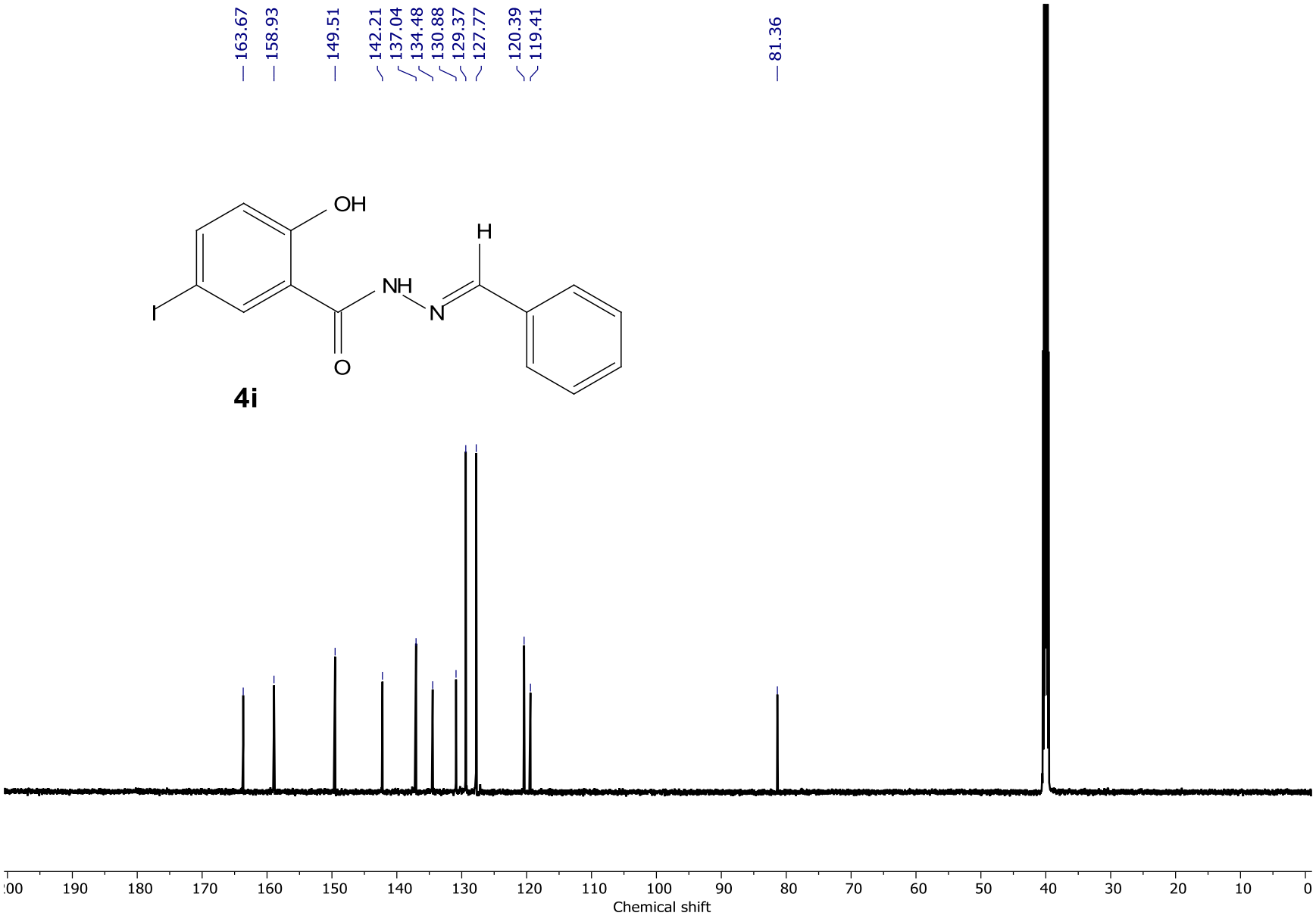
163.67
158.93
149.51
142.21
137.04
134.48
130.88
129.37
127.77
120.39
119.41
81.36
OH
H
NH
N
I
O
4i
Chemical shift

9. References

(1) Frisch, M. J.; Trucks, G. W.; Schlegel, H. B.; Scuseria, G. E.; Robb, M. A.; Cheeseman, J. R.; Scalmani, G.; Barone, V.; Mennucci, B.; Petersson, G. A.; Nakatsuji, H.; Caricato, M.; Li, X.; Hratchian, H. P.; Izmaylov, A. F.; Bloino, J.; Zheng, G.; Sonnenberg, J. L.; Hada, M.; Ehara, M.; Toyota, K.; Fukuda, R.; Hasegawa, J.; Ishida, M.; Nakajima, T.; Honda, Y.; Kitao, O.; Nakai, H.; Vreven, T.; Montgomery, J. A., Jr.; Peralta, J. E.; Ogliaro, F.; Bearpark, M.; Heyd, J. J.; Brothers, E.; Kudin, K. N.; Staroverov, V. N.; Keith, T.; Kobayashi, R.; Normand, J.; Raghavachari, K.; Rendell, A.; Burant, J. C.; Iyengar, S. S.; Tomasi, J.; Cossi, M.; Rega, N.; Millam, J. M.; Klene, M.; Knox, J. E.; Cross, J. B.; Bakken, V.; Adamo, C.; Jaramillo, J.; Gomperts, R.; Stratmann, R. E.; Yazyev, O.; Austin, A. J.; Cammi, R.; Pomelli, C.; Ochterski, J. W.; Martin, R. L.; Morokuma, K.; Zakrzewski, V. G.; Voth, G. A.; Salvador, P.; Dannenberg, J. J.; Dapprich, S.; Daniels, A. D.; Farkas, Ö.; Foresman, J. B.; Ortiz, J. V.; Cioslowski, J.; Fox, D. J. Gaussian 09, Revision D.01; Gaussian, Inc.: Wallingford, CT, 2010.

(2) Chai, J.-D.; Head-Gordon, M. Long-Range Corrected Hybrid Density Functionals with Damped Atom–Atom Dispersion Corrections. *Phys. Chem. Chem. Phys.* **2008**, *10* (44), 6615–6620. https://doi.org/10.1039/b810189b

(3) Weigend, F.; Ahlrichs, R. Balanced Basis Sets of Split Valence, Triple Zeta Valence and Quadruple Zeta Valence Quality for H to Rn: Design and Assessment of Accuracy. *Phys. Chem. Chem. Phys.* **2005**, *7* (18), 3297–3305. https://doi.org/10.1039/b508541a

(4) Nielsen, A. B.; Holder, A. J. GaussView 5.0, User's Reference; Gaussian Inc.: Pittsburgh, PA, 2009.

(5) Sim, L., Quezada-Calvillo, R., Sterchi, E. E., Nichols, B. L., & Rose, D. R. (2008). Human Intestinal Maltase–Glucoamylase: Crystal Structure of the N-Terminal Catalytic Subunit and Basis of Inhibition and Substrate Specificity. *Journal of Molecular Biology*, *375*(3), 782-792. https://doi.org/10.1016/j.jmb.2007.10.069

(6) Mats H. M. Olsson, Chresten R. Søndergaard, Michal Rostkowski, and Jan H. Jensen. (2011) PROPKA3: Consistent Treatment of Internal and Surface Residues in Empirical pKa Predictions. Journal of Chemical Theory and Computation ***2011*** 7 *(2), 525-537.* https://doi.org/10.1021/ct100578z

(7) Jorgensen, W. L., Maxwell, D. S., & Tirado-Rives, J. (1996). Development and Testing of the OPLS All-Atom Force Field on Conformational Energetics and Properties of Organic Liquids. *Journal of the American Chemical Society*, *118*(45), 11225–11236. https://doi.org/10.1021/ja9621760

(8) McNutt, A. T., Francoeur, P., Aggarwal, R., Masuda, T., Meli, R., Ragoza, M., Sunseri, J., & Koes, D. R. (2021). GNINA 1.0: molecular docking with deep learning. *Journal of Cheminformatics*, *13*(1), 43. https://doi.org/10.1186/s13321-021-00522-2

(9) Quiroga, R., & Villarreal, M. A. (2016). Vinardo: A Scoring Function Based on Autodock Vina Improves Scoring, Docking, and Virtual Screening. *PLOS ONE*, *11*(5), e0155183. https://doi.org/10.1371/journal.pone.0155183